AIDAA Educational Series & Academy

Università degli Studi di Enna “Kore”
Facoltà di Ingegneria e Architettura

Sound transmission control through optimized composite sandwich lattice panels

8, 15, 22, 29 October 2021
15:00 – 17:00 CEST

Contributors:
Dr. Stefano Valvano, Prof. Calogero Orlando

Webinar organization

Webinar	Speaker	Date	Time
Sound transmission: Introduction and Modeling approach	Orlando/ Valvano	October 8	15:00-17:00
Structural models for Damping Lattice-Core Sandwich Panels	Valvano	October 15	15:00-17:00
Population Decline Swarm Optimizer	Orlando	October 22	15:00-17:00
Sound transmission analysis of optimized composite sandwich lattice panels	Valvano	October 29	15:00-17:00

Outline

- Sound transmission study of a fuselage section
- Sound transmission evaluation: sound parameters
- Structural models for multilayered structures in aeronautics
- Viscoelastic materials as passive damper
- Lattice cell structure for aeronautical sandwich panels

Sound transmission study of a fuselage section

CAD model sketch of an hypothetical regional aircraft fuselage trunk and selecting a circular section model with four seats for sitting.

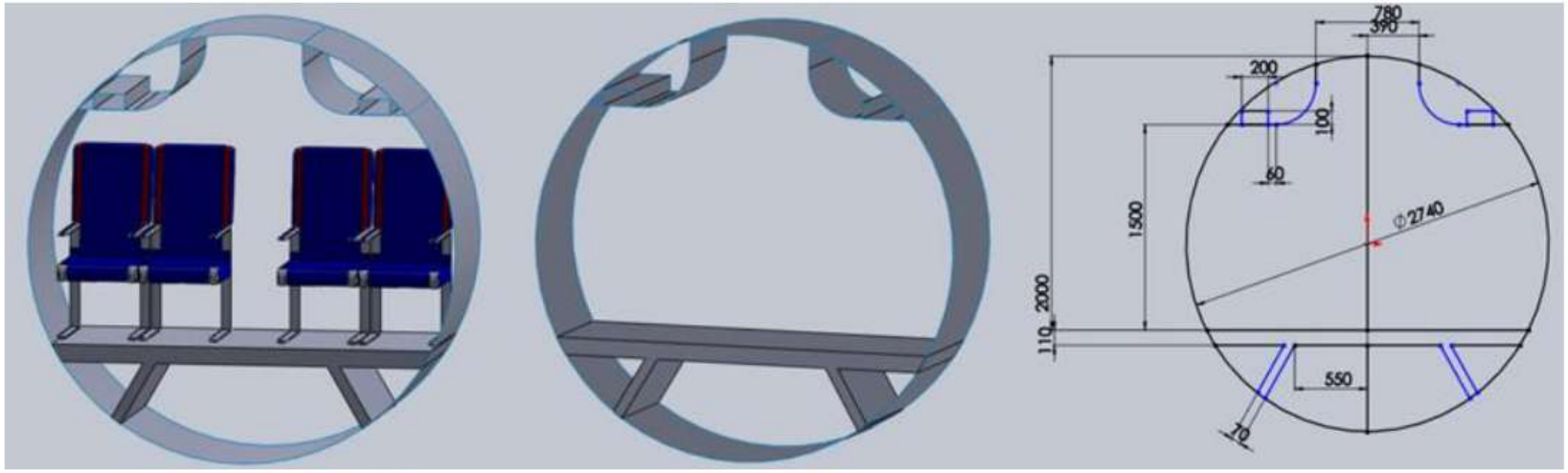

Fig. 2 CAD model of the fuselage trunk (dimensions are given in [mm])

Cinefra, M., Passabi, S., & Carrera, E. (2018). FEM vibroacoustic analysis in the cabin of a regional turboprop aircraft. Advances in aircraft and spacecraft science, 5(4), 477.

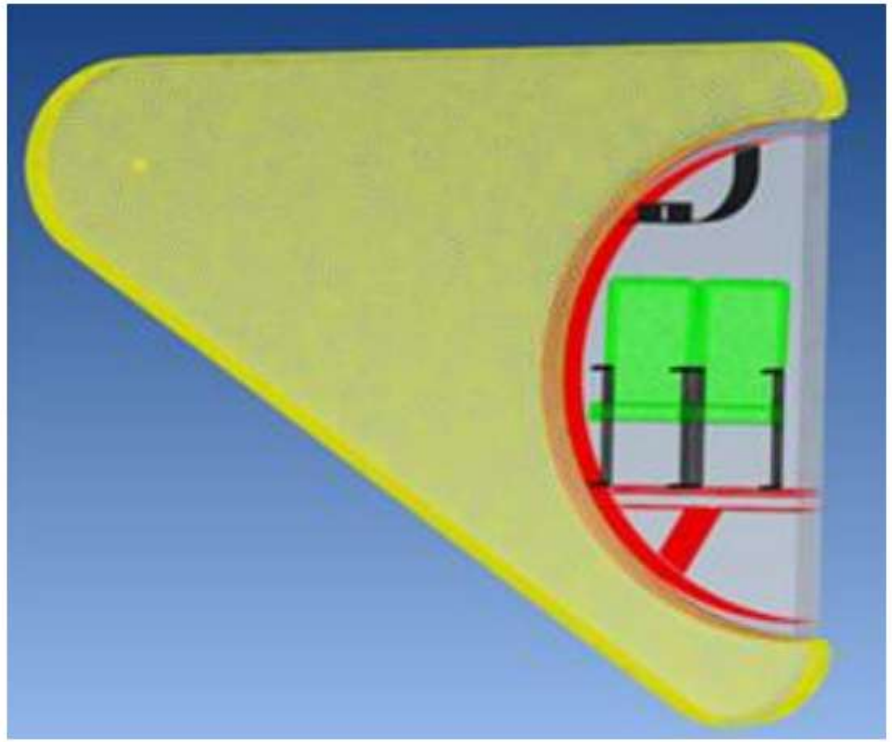

Fig. 7 Fuselage trunk with sound spherical source

Apex MSC Software transformed the CAD file into a mesh file recognizable by Actran. The model consists in 2420 1D elements, 177329 2D elements, 478375 3D elements and 384014 nodes.

The spherical source simulates the presence of an engine , positioned under the wing of a turboprop aircraft with high wing configuration. It must be supported by a volume mesh. This volume identifies the air around the engine and the air inside the cabin, as means of propagation of sound.

Cinefra, M., Passabi, S., & Carrera, E. (2018). FEM vibroacoustic analysis in the cabin of a regional turboprop aircraft. Advances in aircraft and spacecraft science, 5(4), 477.

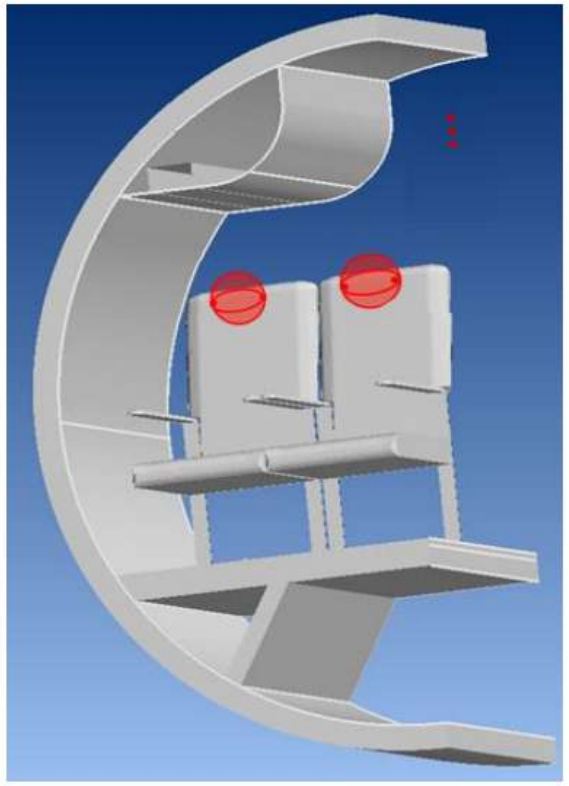

Fig. 8 Microphones positions

In the model, there are multiple point load and microphones which detect the number of decibels inside the fuselage. Since the number of microphones is high, the different regions are computed using the mean quadratic pressure.

These are positioned as follows:
- three at standing position in the isle, taking into account the average height of the European population (center corridor 1.65 m, 1.70 m and 1.75 m from the floor);
- two at ears positions for the window seat;
- two at ears positions for the isle seat;
- a sphere microphone for the possible head movement at the window seat;
- a sphere microphone for the possible head movement at the isle seat.

Cinefra, M., Passabi, S., & Carrera, E. (2018). FEM vibroacoustic analysis in the cabin of a regional turboprop aircraft. Advances in aircraft and spacecraft science, 5(4), 477.

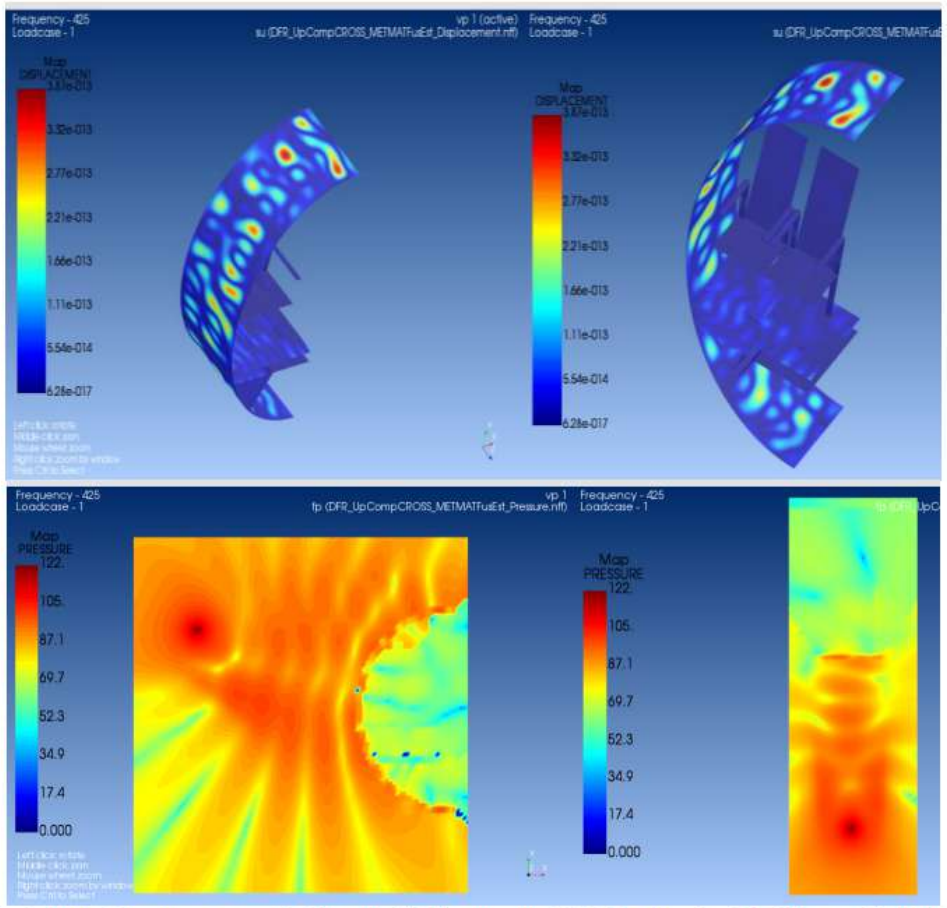

Fig. 9 (up) Output map and (down) field map at 425 Hz for the META configuration

Output map associated to the domains of the fuselage, floor and reinforcement that provides information about the displacements of the structure.

Field map associated to a longitudinal and transversal plane that provides the variation of pressure level sound across the fuselage

Cinefra, M., Passabi, S., & Carrera, E. (2018). FEM vibroacoustic analysis in the cabin of a regional turboprop aircraft. Advances in aircraft and spacecraft science, 5(4), 477.

Fuselage configurations

- Upper engine aluminum internal fuselage (**UAFI**): In this study case, a **single aluminum layer** of 1 mm thickness was assigned to the fuselage.
- Upper engine composite internal fuselage (**UCFI**): The properties of the **composite material** are taken directly from the database of Actran software. A **single internal layer** of fuselage is considered.
- Upper engine cross-ply composite internal fuselage (**UCCFI**): In this configuration, the **cross-ply composite material** has been associated to the items that in the previous configuration were made with Actran composite.
- Upper engine cross-ply composite enternal fuselage (**UCCFE**): In this case, the same configuration of the previous case has been used, but the **outer layer of the fuselage is included**. The cross-ply composite is assigned also to the outer layer and **an acoustic volume of air** has been associated to the volume **included between the two shells of the fuselage wall**.
- Upper engine cross-ply composite with polymide external fuselage (**META**): This particular configuration has been analyzed in order to test the absorption properties of a new porous material, such as the Polymide. **The Polymide substitutes the volume of air between the two cross-ply composite layers in the previous model**. In this way, a sort of sandwich structure is obtained with very stiff skins and a viscoelastic soft core. This last, being porous, provide a good sound absorption at high frequencies.

Cinefra, M., Passabi, S., & Carrera, E. (2018). FEM vibroacoustic analysis in the cabin of a regional turboprop aircraft. Advances in aircraft and spacecraft science, 5(4), 477.

Microphones of isle: In this condition, one can note that for low frequencies, up to 400 Hz, the chosen materials keep a limit level of sound pressure level of 76,5 dBA (74 dBA + 2,5 dBA due to the wing effect). This level is acceptable for a good acoustic comfort in the cabin, but the composite materials fail to maintain a sufficiently low noise level over the 865 Hz.

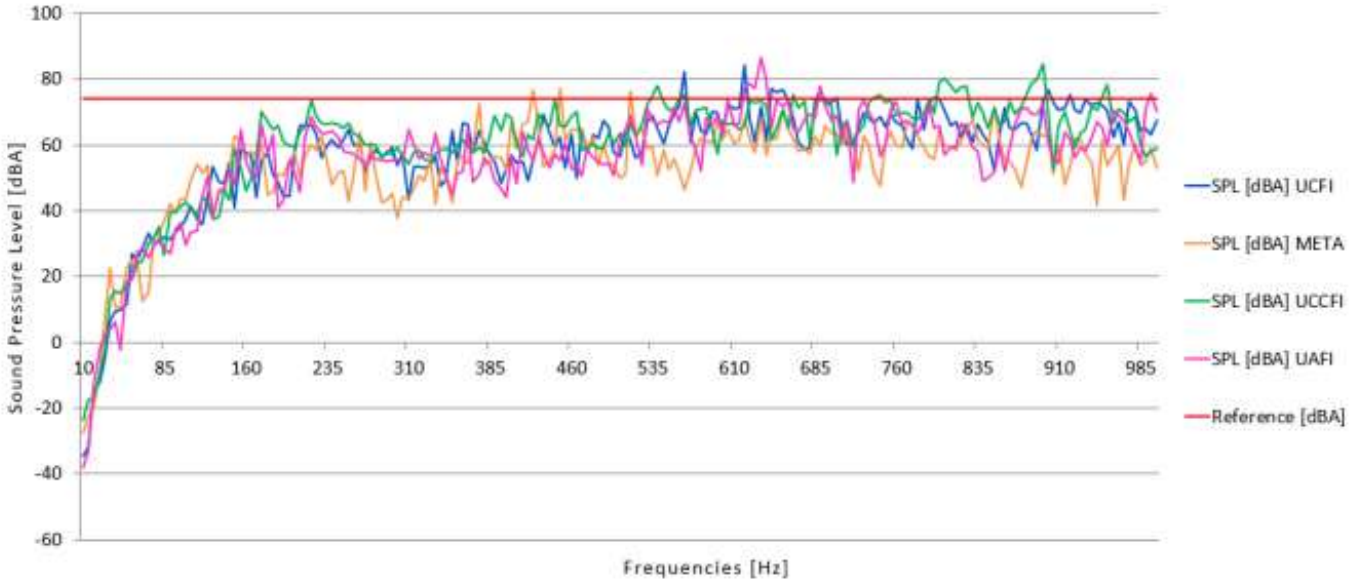

Fig. 10 Trend of sound pressure level in the isle

Each material behaves differently depending on the frequencies: the porous material does not respond well at medium-low frequencies of 415 and 525 Hz. The highest peaks occur in the aluminum fuselage at 635 Hz and for the cross-ply fuselage at 895 Hz. In general, the results with lower trends are given by aluminum or porous material.

Cinefra, M., Passabi, S., & Carrera, E. (2018). FEM vibroacoustic analysis in the cabin of a regional turboprop aircraft. Advances in aircraft and spacecraft science, 5(4), 477.

Microphones at ears of window seat: The results do not change much with respect to the previous case. One can immediately note that the configurations with composite materials tend to exceed the limit of 74 dBA at 815 Hz for the UFCCI configuration and 915 Hz for the UFCI one.

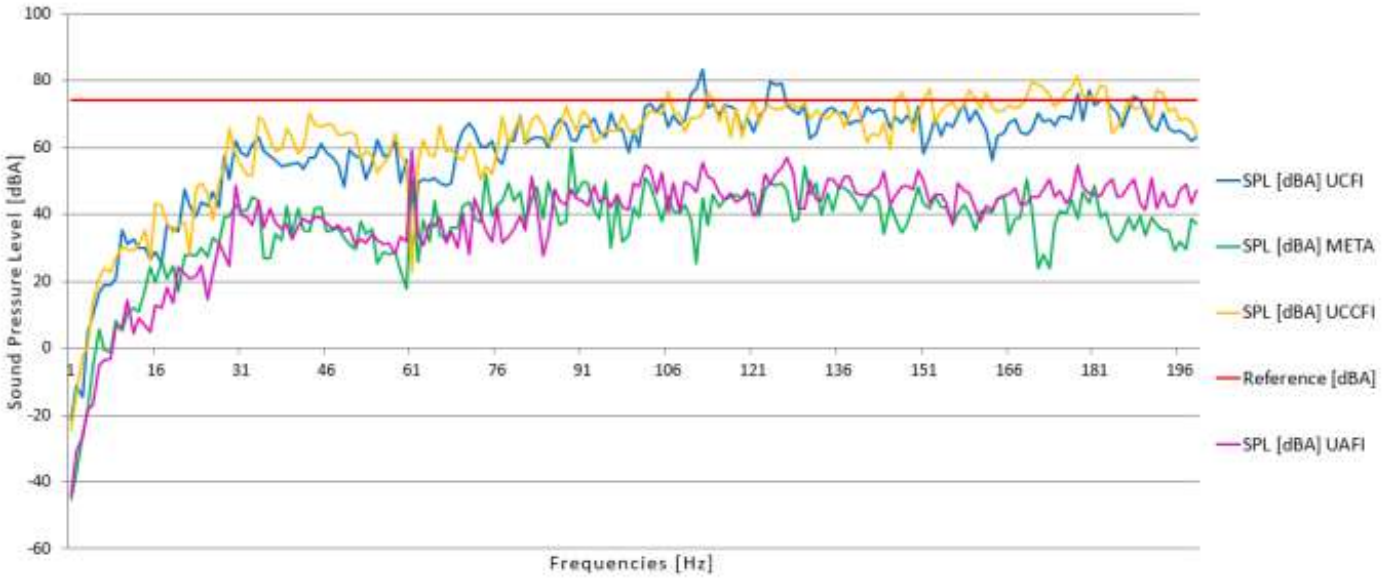

Fig. 11 Trend of sound pressure level at the ears of the window seat

The lower sound pressure levels are obtained META configuration followed by the fuselage of aluminum. This last two materials do not present resonance peaks over 76,5 dBA, while the UFCI shows resonance peaks at 625 and 905 Hz and the UFCCI at 535 and 895.

Cinefra, M., Passabi, S., & Carrera, E. (2018). FEM vibroacoustic analysis in the cabin of a regional turboprop aircraft. Advances in aircraft and spacecraft science, 5(4), 477.

Sound transmission evaluation: sound parameters

In order to evaluate the sound pressure transmitted through a panel, such as a fuselage panel, it it possible to consider the vibration characteristics of the considered structures as a source and to evaluate the sound pressure field by the use of the Rayleigh integral relation as follows:

$$p(x,y,z,\omega) = \frac{\rho_{air} j\omega}{2\pi} \int_{\Omega} v_n(x',y',0,\omega) \frac{e^{-jkR}}{R} \, d\Omega$$

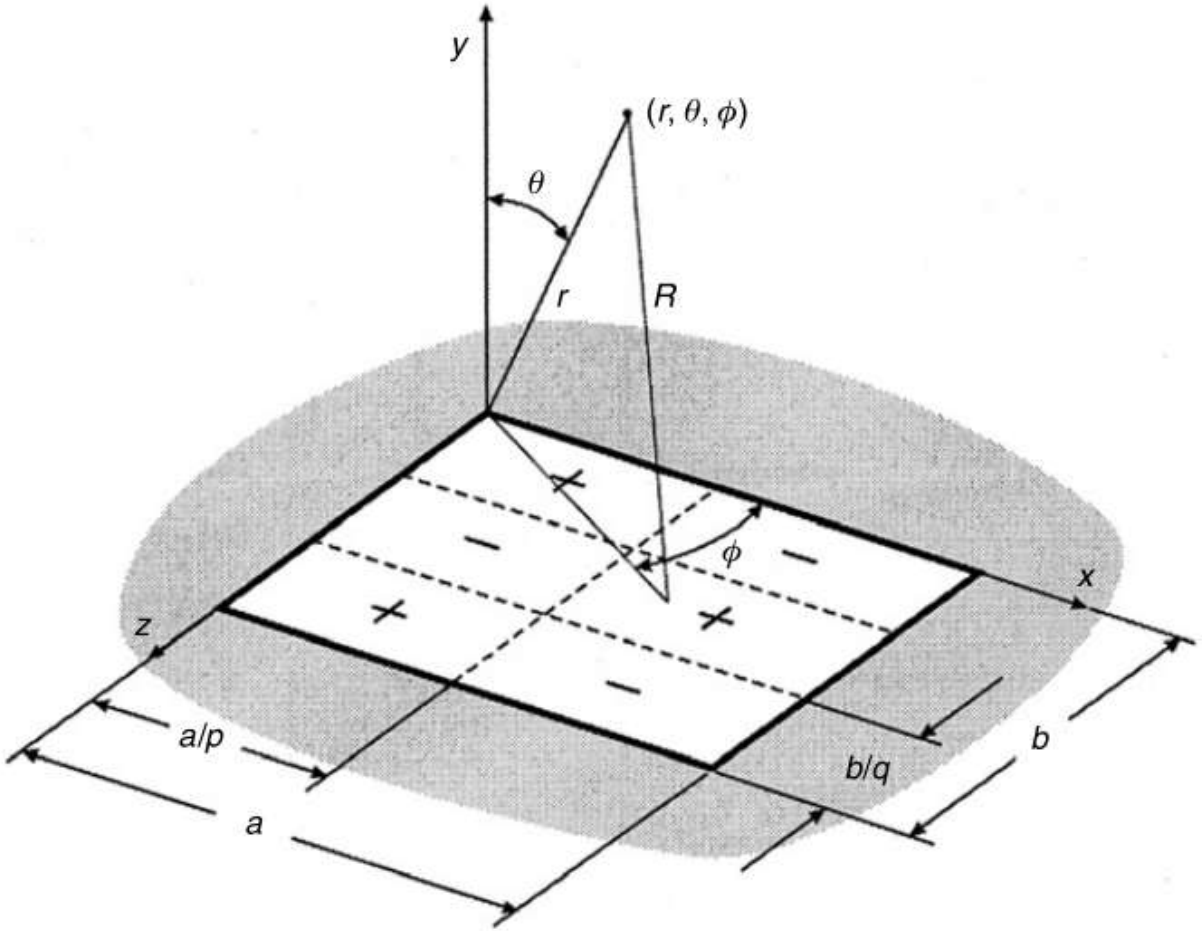

Fig. 3.7. Coordinate system, nodal lines and phases of a vibrating rectangular panel.

The distance R is evaluated between the evaluation point and each vibrating source point/region as follows:

$$R = \sqrt{(x - x')^2 + (y - y')^2 + (z - 0)^2}$$

Fahy, F. J., & Gardonio, P. (2007). Sound and structural vibration: radiation, transmission and response. Elsevier.

Meanwhile the sound pressure field is a local variable, dependent on the evaluation point (x,y,z), differently, it is possible to define a global variable, the emitted sound power defined as follows:

$$\Pi_t(\omega) = \frac{1}{2}\Re\left(\int_\Omega p(x,y,0,\omega)\overline{v}_n(x,y,0,\omega)\,d\Omega\right)$$

Although the formulation presented above seems to be quite simple and neat, the evaluation of the sound power is related to the derivation of the quadruple integrals (a surface integral for the sound pressure field and another surface integral for the sound power). An alternative approach based on the elementary radiators is proposed.

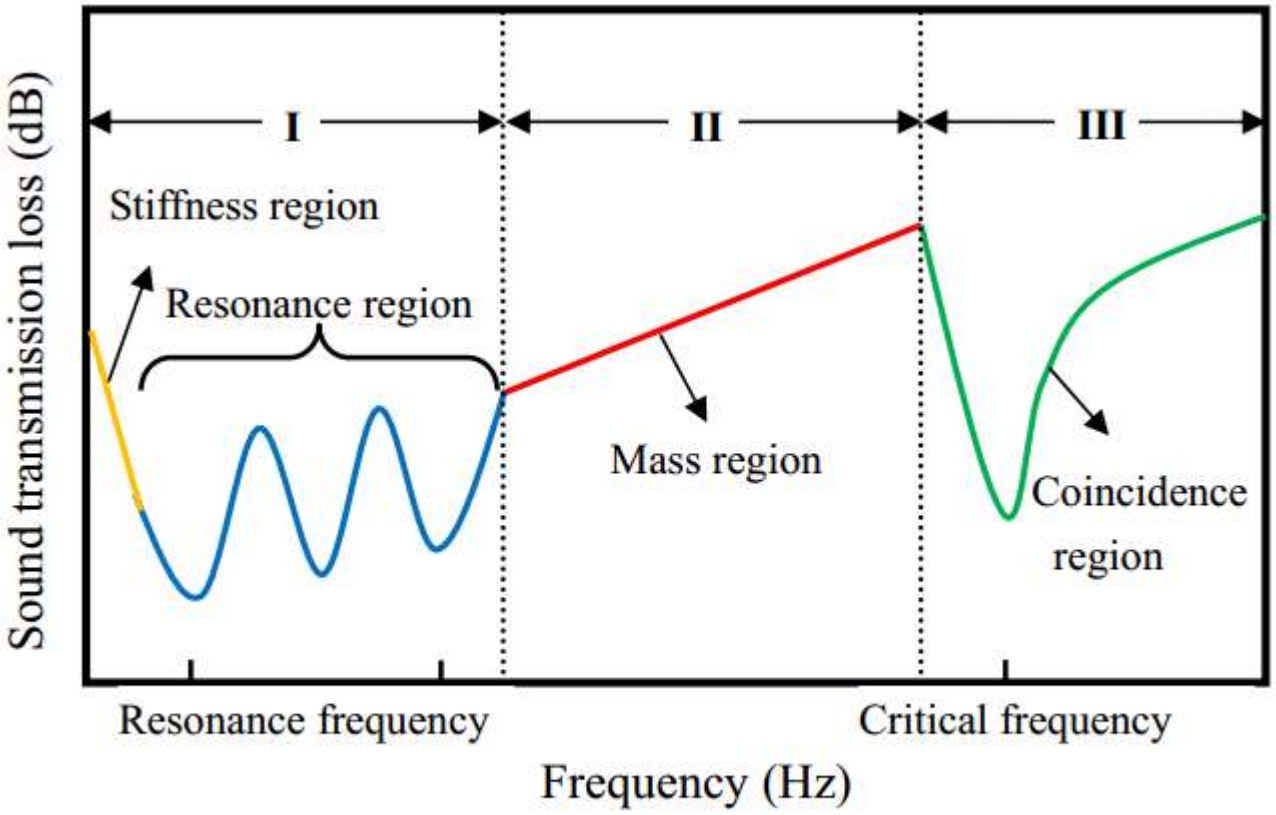

Fig. 1. The STL curve controlled by various region.

Sound transmission levels are clearly related to the vibration characteristics of the considered structure. It is well known from the literature that the STL is driven by the stiffness and mass properties in different parts of the spectra. As a consequence, it is clear that the stiffness and mass properties could be tuned in a proper way in the design process of a structure.

Yang, Y. et al. (2016). Acoustic properties of glass fiber assembly-filled honeycomb sandwich panels. Composites Part B: Engineering, 96, 281-286.

Structural models for multilayered structures in aeronautics

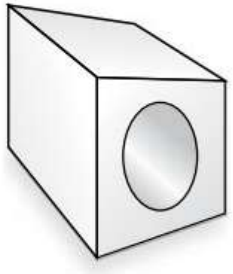

Figure 1.1 Example of 3D structure

Figure 1.2 Example of 2D structure

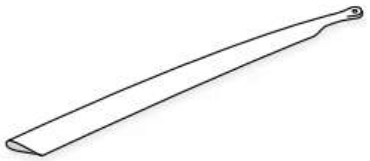

Figure 1.3 Example of 1D structure (helicopter blade)

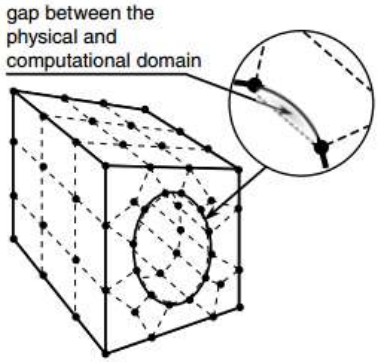

Figure 1.4 Example of a 3D FEM model

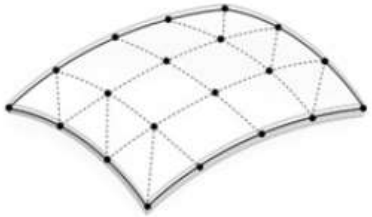

Figure 1.5 Example of 2D FEM model

Figure 1.6 Example of 1D FEM model

Different theoretical approach can be used for the the structural analysis. The choice is related to the geometrical complexity and properties of the considered structure.

Carrera, E., Cinefra, M., Petrolo, M., & Zappino, E. (2014). Finite element analysis of structures through unified formulation. John Wiley & Sons.

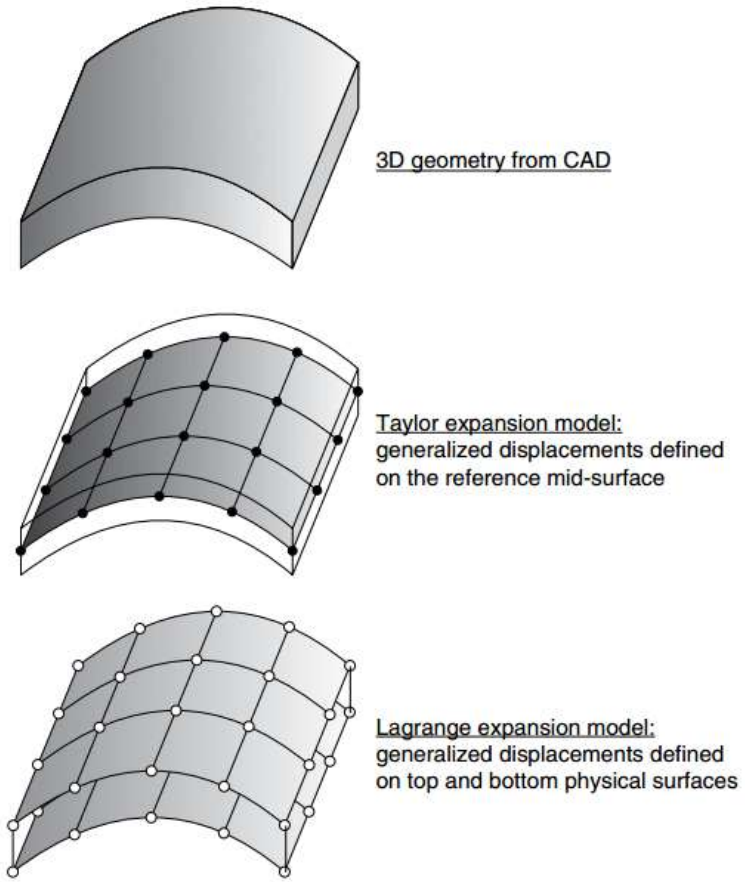

Figure 12.1 Different geometrical modelling approaches, TE model vs LE model

Shell panel modelization, finite elements with classical Taylor expansion models, and advanced Lagrange thickness models.

Carrera, E., Cinefra, M., Petrolo, M., & Zappino, E. (2014). Finite element analysis of structures through unified formulation. John Wiley & Sons.

Classical Lamination Theory:
Geometrical representation and kinematic displacement field.

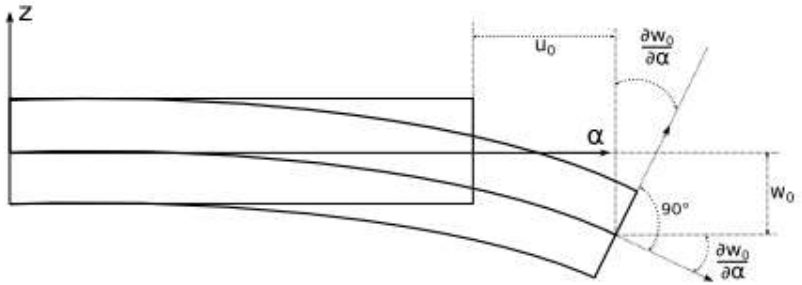

Figure 3.1: Geometrical representation of the Kirchoff’s assumptions.

$$
\begin{aligned}
u(\alpha,\beta,z) &= u_0(\alpha,\beta) - z\frac{\partial w_0}{\partial \alpha} \\
v(\alpha,\beta,z) &= v_0(\alpha,\beta) - z\frac{\partial w_0}{\partial \beta} \\
w(\alpha,\beta,z) &= w_0(\alpha,\beta)
\end{aligned}
\tag{3.1}
$$

Carrera, E., Pagani, A., & Valvano, S. (2017). Multilayered plate elements accounting for refined theories and node-dependent kinematics. Composites Part B: Engineering, 114, 189-210.

First-order Shear Deformation Theory:
Geometrical representation and kinematic displacement field.

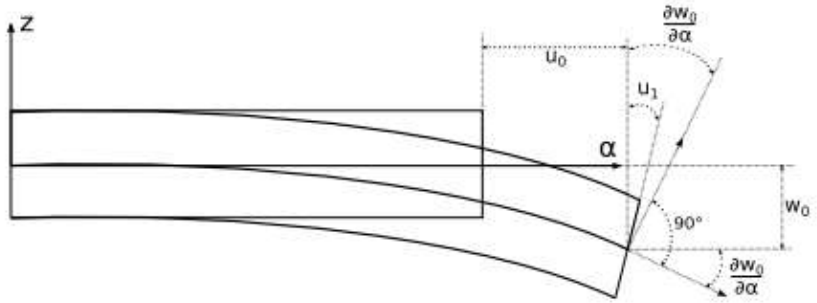

Figure 3.2: Geometrical rapresentation of the Reissner-Mindlin theory.

$$
\begin{aligned}
u(\alpha,\beta,z) &= u_0(\alpha,\beta) + z\,u_1(\alpha,\beta) \\
v(\alpha,\beta,z) &= v_0(\alpha,\beta) + z\,v_1(\alpha,\beta) \qquad (3.2) \\
w(\alpha,\beta,z) &= w_0(\alpha,\beta)
\end{aligned}
$$

Carrera, E., Pagani, A., & Valvano, S. (2017). Multilayered plate elements accounting for refined theories and node-dependent kinematics. Composites Part B: Engineering, 114, 189-210.

Higher-Order Theories:
Geometrical representation and kinematic displacement field.

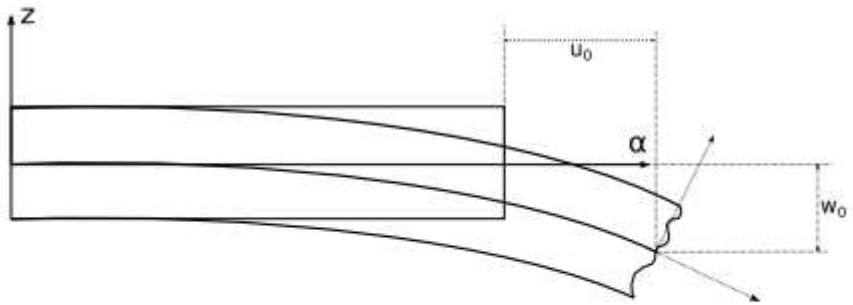

Figure 3.3: Geometrical representation of the Higher Order Theories.

$$
\begin{aligned}
u(\alpha,\beta,z) &= u_0(\alpha,\beta) + z\,u_1(\alpha,\beta) + \ldots + z^N\,u_N(\alpha,\beta)\\
v(\alpha,\beta,z) &= v_0(\alpha,\beta) + z\,v_1(\alpha,\beta) + \ldots + z^N\,v_N(\alpha,\beta)\\
w(\alpha,\beta,z) &= w_0(\alpha,\beta) + z\,w_1(\alpha,\beta) + \ldots + z^N\,w_N(\alpha,\beta)
\end{aligned}
\tag{3.3}
$$

Carrera, E., Pagani, A., & Valvano, S. (2017). Multilayered plate elements accounting for refined theories and node-dependent kinematics. Composites Part B: Engineering, 114, 189-210.

Multilayered panel sketch, **Equivalent-Single-Layer (ESL)** modeling approach for different expansion orders.

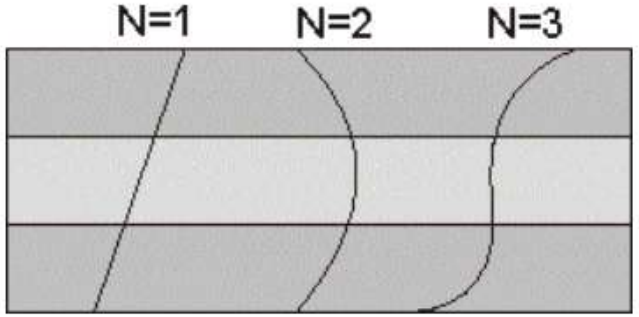

Figure 3.4: Equivalent-Single-Layer behaviour of the primary variables along the thickness of the shell.

Valvano, S. (2017). Development of computational efficient shell formulation for analysis of multilayered structures subjected to mechanical, thermal, and electrical loadings (Doctoral dissertation, Ph. D. Thesis, Politecnico di Torino, Turin, Italy).

$$u^k(x,y,z,t) = \sum_{j=1}^{m} u_j^k(x,y,t)\phi_j^k(z)$$

$$v^k(x,y,z,t) = \sum_{j=1}^{m} v_j^k(x,y,t)\phi_j^k(z)$$

$$w^k(x,y,z,t) = \sum_{j=1}^{n} w_j^k(x,y,t)\psi_j^k(z)$$

In the layerwise theory of Reddy, the displacements of the kth layer are written using selected layerwise continuous functions. They can be chosen to be the one-dimensional Lagrange interpolation functions of the thickness coordinate.

Reddy, J. N., (1997). Mechanics of laminated composite plates and shells: theory and analysis. CRC press.

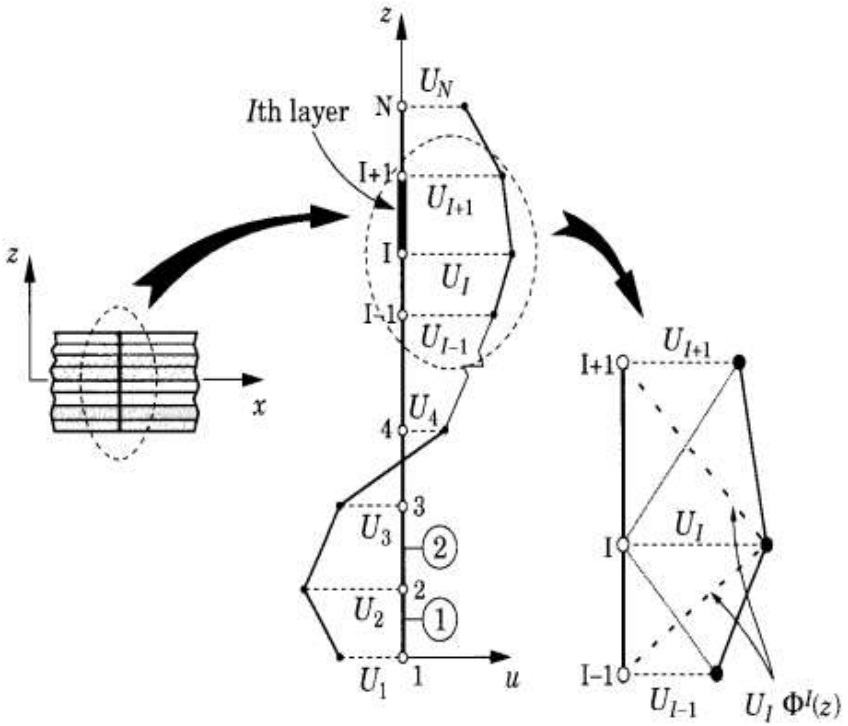

Figure 12.2.1: Displacement representation and the linear approximation functions $\Phi^I(z)$ used in the layerwise theory.

Any desired degree of displacement variation through the thickness is easily obtained using higher order Lagrangian interpolation polynomials through the thickness.

Reddy, J. N., (1997). Mechanics of laminated composite plates and shells: theory and analysis. CRC press.

$$\mathbf{u}(x, y, z) = F_\tau(z)\mathbf{u}_\tau(x, y), \qquad \tau = 0, 1, \ldots, N$$

$$u_\alpha = F_t\, u_{\alpha_t} + F_b\, u_{\alpha_b}$$
$$u_\beta = F_t\, u_{\beta_t} + F_b\, u_{\beta_b}$$
$$u_z = F_t\, u_{z_t} + F_b\, u_{z_b}$$

$$F_t = \frac{1+\zeta}{2}$$
$$F_b = \frac{1-\zeta}{2}$$

Layer-Wise kinematic expansion models can be described in a general framework of kinematic structural theories known as Unified Formulation by Carrera (CUF).

Carrera, E., Cinefra, M., Petrolo, M., & Zappino, E. (2014). Finite element analysis of structures through unified formulation. John Wiley & Sons.

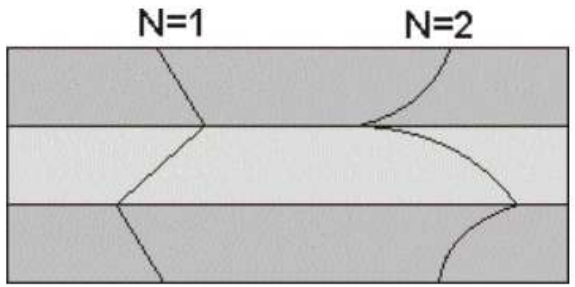

Figure 3.5: Layer-Wise behaviour of the primary variables along the thickness of the shell.

Multilayered panel sketch, **Layer-Wise (LW)** modeling approach for different expansion orders.

The displacement variables continuity is directly ensured at each interface layer.

$$\boldsymbol{u}_t^k = \boldsymbol{u}_b^{k+1}, \qquad k = 1, N_l - 1.$$

Valvano, S. (2017). Development of computational efficient shell formulation for analysis of multilayered structures subjected to mechanical, thermal, and electrical loadings (Doctoral dissertation, Ph. D. Thesis, Politecnico di Torino, Turin, Italy).

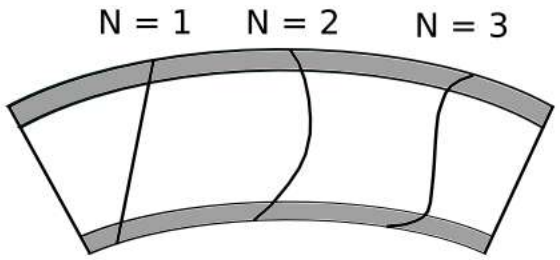

Figure 9.1: Equivalent-Single-Layer behaviour of the primary variables along the thickness of the shell.

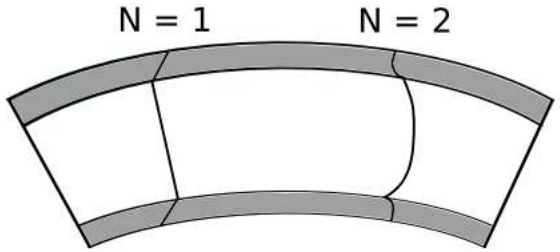

Figure 9.3: Layer-Wise behaviour of the primary variables along the thickness of the shell.

Sandwich panels assembling approaches: **Equivalent-Single-Layer** and **Layer-Wise** modeling approaches for different expansion orders.

Valvano, S. (2017). Development of computational efficient shell formulation for analysis of multilayered structures subjected to mechanical, thermal, and electrical loadings (Doctoral dissertation, Ph. D. Thesis, Politecnico di Torino, Turin, Italy).

Sandwich panels static analysis

The static analysis of a sandiwch panel structure is performed by the use of the Principle of Virtual Displacements (**PVD**).

$$\int_{\Omega} \int_{A} \delta \boldsymbol{\epsilon}^T \boldsymbol{\sigma} \, d\Omega \, dz = \delta L_e$$

The governing equations can be derived in compact form:

$$\delta \boldsymbol{u}_{\tau_i} : \quad \boldsymbol{K}^{\tau s ij} \boldsymbol{u}_{s_j} = \quad \boldsymbol{P}^{\tau i}$$

Geometrical sketch of a quarter of the sandwich panel loaded by a localized uniform pressure.

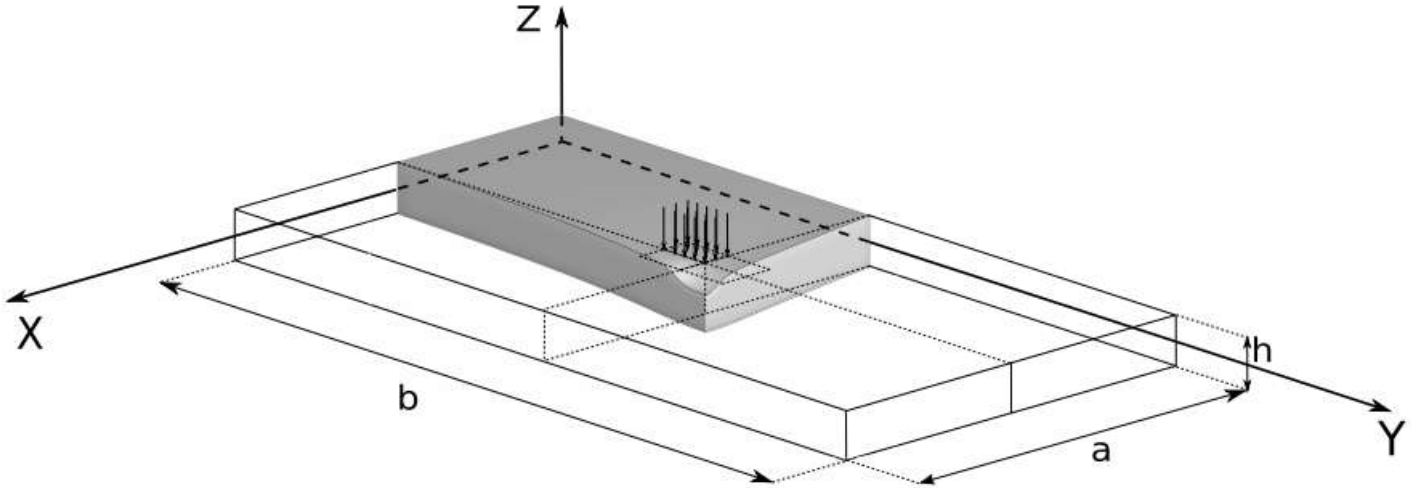

Figure 10.29: Reference system of the sandwich plate. Three-dimensional deflection representation of a quarter of the plate.

Valvano, S., & Carrera, E. (2017). Multilayered plate elements with node-dependent kinematics for the analysis of composite and sandwich structures. Facta Universitatis, Series: Mechanical Engineering, 15(1), 1-30.

Table 10.7: Unsymmetrically laminated rectangular sandwich plate. Transverse displacement w, in-plane normal stresses σ_{xx} and σ_{yy}, and transverse normal stress σ_{zz} evaluated at $(a/2, b/2)$ by various single- and multi-theory models.

	z	w	σ_{xx}	σ_{yy}	σ_{zz}	$DOFs$
		Top Skin				
3D Analytical [182]	Top	-3.78	-624	-241	-	
	Bottom		580	211	-	
3D NASTRAN [182]	Top	-3.84	-628	-237	-	
	Bottom		582	102	-	
LWM2 Analytical [183]	Top	-3.8243	-619.49	-	-	
	Bottom		577.36	-	-	
LWM2 FEM [184]	Top	-3.7628	-595.56	-223.93	-	
	Bottom		556.00	196.37	-	
		Top Skin				
$LW4$	Top	-3.7774	-622.48	-233.39	-0.9649	327327
	Bottom		578.60	203.25	-0.8738	
$LW3$	Top	-3.7723	-618.14	-232.33	-1.0143	251790
	Bottom		574.87	202.36	-0.8270	
$LW2$	Top	-3.7552	-601.46	-228.13	-0.9813	176253
	Bottom		559.72	198.73	-0.8710	
$LW1$	Top	-3.3896	-562.86	-286.15	-242.69	100716
	Bottom		530.98	262.78	240.82	
$ET4$	Top	-2.5498	-248.99	-38.930	256.87	125895
	Bottom		184.89	-1.7709	-275.80	
$ET3$	Top	-0.5995	-121.19	-56.428	-21.706	100716
	Bottom		59.439	8.9946	-19.349	
$ET2$	Top	-0.0238	-29.573	-28.178	-30.655	75537
	Bottom		-27.989	-27.470	-29.934	
$ET1$	Top	-0.0191	-29.740	-25.448	-25.404	50358
	Bottom		-29.444	-25.211	-25.248	
Case A	Top	-2.1386	-622.21	-220.95	-0.9649	245619
	Bottom		567.44	198.35	-0.8738	
Case B	Top	-2.4177	-609.14	-217.40	-0.9654	161007
	Bottom		563.79	196.16	-0.8663	

Transverse displacement and normal stresses evaluated for different ESL and LW theories.

LW models permit to reach accurate results with respect to ESL models.

Valvano, S., & Carrera, E. (2017). Multilayered plate elements with node-dependent kinematics for the analysis of composite and sandwich structures. Facta Universitatis, Series: Mechanical Engineering, 15(1), 1-30.

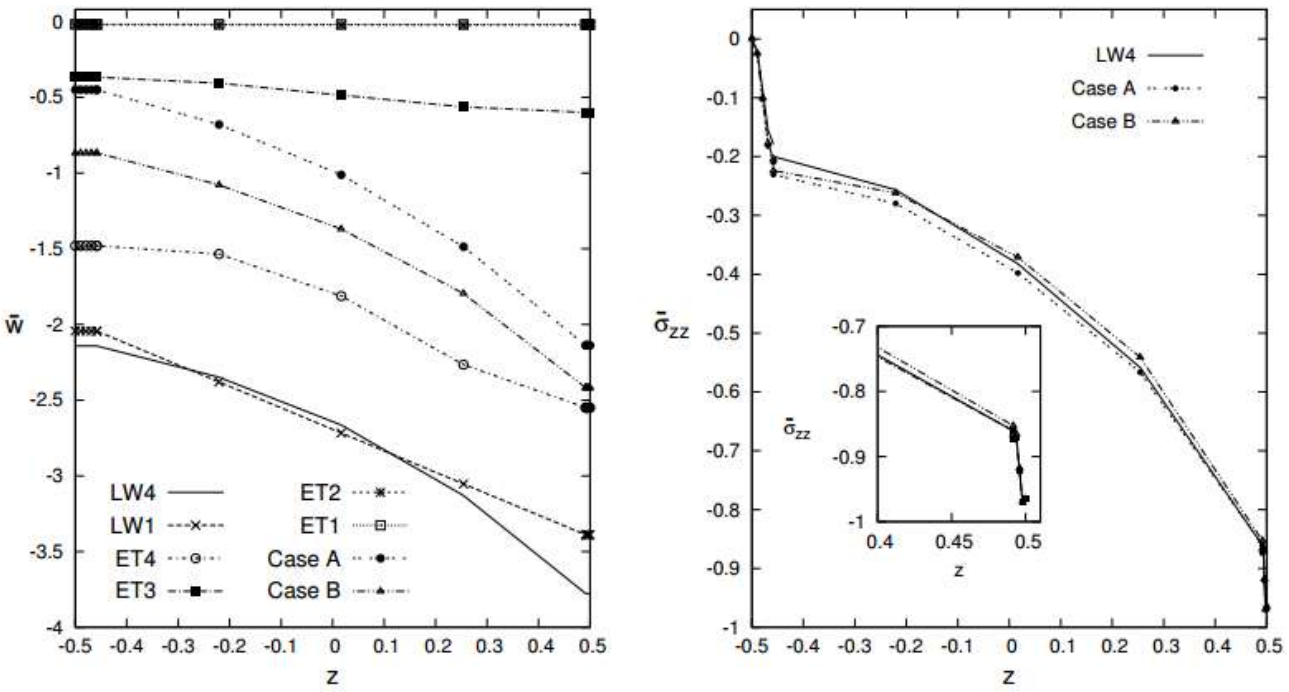

Figure 10.31: Unsymmetrically laminated rectangular sandwich plate. Transverse displacement $w(x;y)$, and transverse normal stress $\sigma_{zz}(x;y)$ evaluated at $(a/2, b/2)$ by various single- and multi-theory models.

Transverse displacement and normal stress behavior through the thickness for different LW and ESL theories.

Valvano, S., & Carrera, E. (2017). Multilayered plate elements with node-dependent kinematics for the analysis of composite and sandwich structures. Facta Universitatis, Series: Mechanical Engineering, 15(1), 1-30.

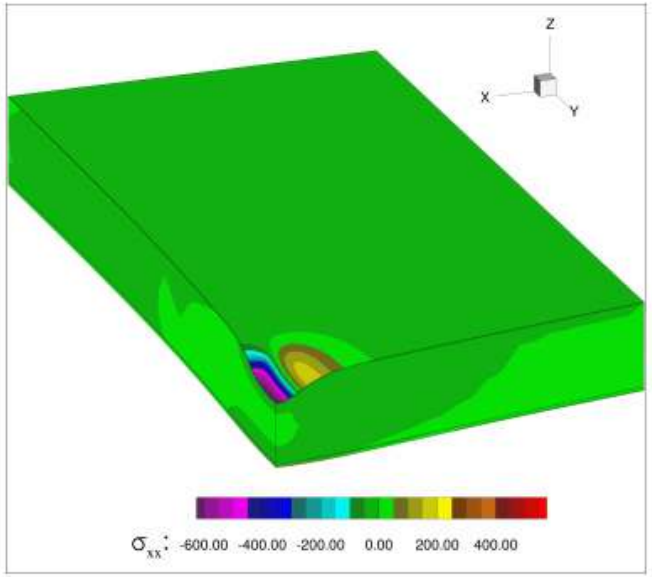

(a) $LW4$

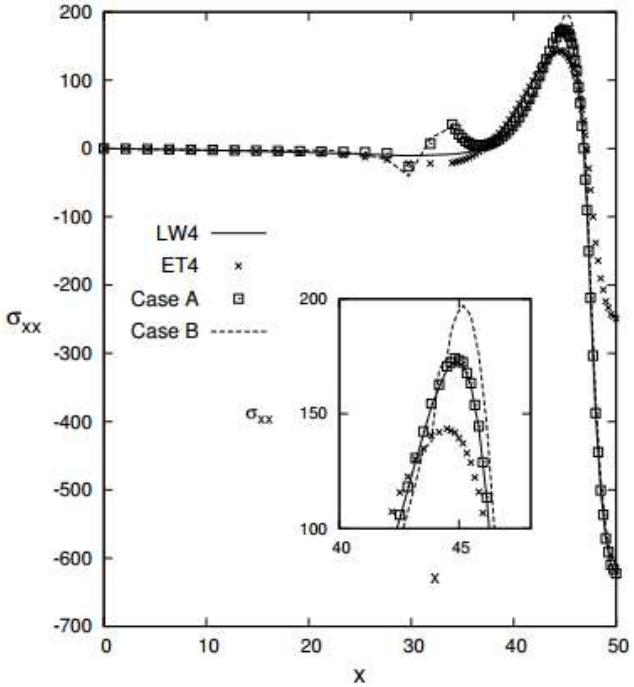

(b) Single and multi-models.

Figure 10.32: Unsymmetrically laminated rectangular sandwich plate. In-plane stress σ_{xx}, three-dimensional view of a quarter of the plate, and in-plane stress along the in-plane axis direction X evaluated at $(y, z) = (b/2, +h/2)$, for single and multi-models.

In-plane normal stress three-dimensional representation on a quarter of the sandwich panel and in-plane normal stress through the X direction for different LW and ESL models.

Valvano, S., & Carrera, E. (2017). Multilayered plate elements with node-dependent kinematics for the analysis of composite and sandwich structures. Facta Universitatis, Series: Mechanical Engineering, 15(1), 1-30.

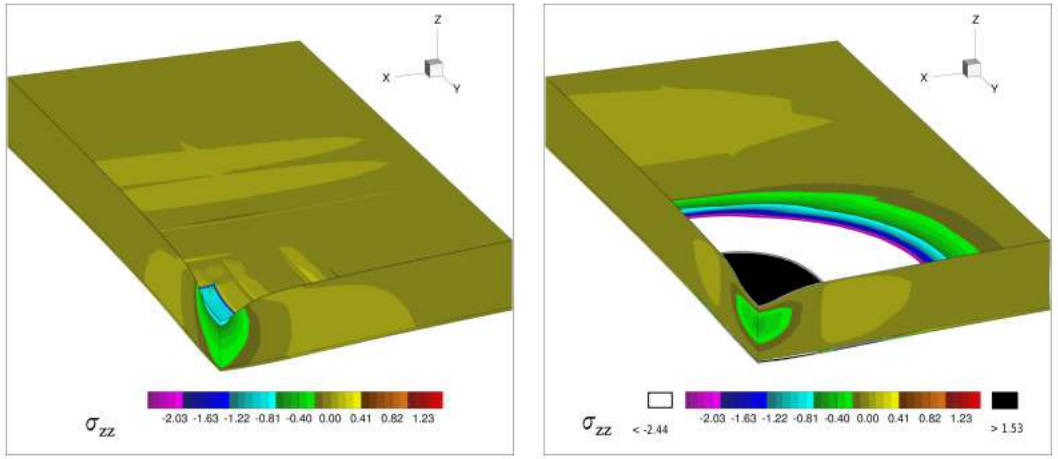

(a) $LW4$ (b) $ET4$

Figure 10.33: Unsymmetrically laminated rectangular sandwich plate, three-dimensional view of a quarter of the plate. Transverse normal stress σ_{zz} for single models.

Thickness normal stress three-dimensional representation on a quarter of the sandwich panel for the LW4 and ET4 theories.

Valvano, S., & Carrera, E. (2017). Multilayered plate elements with node-dependent kinematics for the analysis of composite and sandwich structures. Facta Universitatis, Series: Mechanical Engineering, 15(1), 1-30.

Viscoelastic materials as passive damper

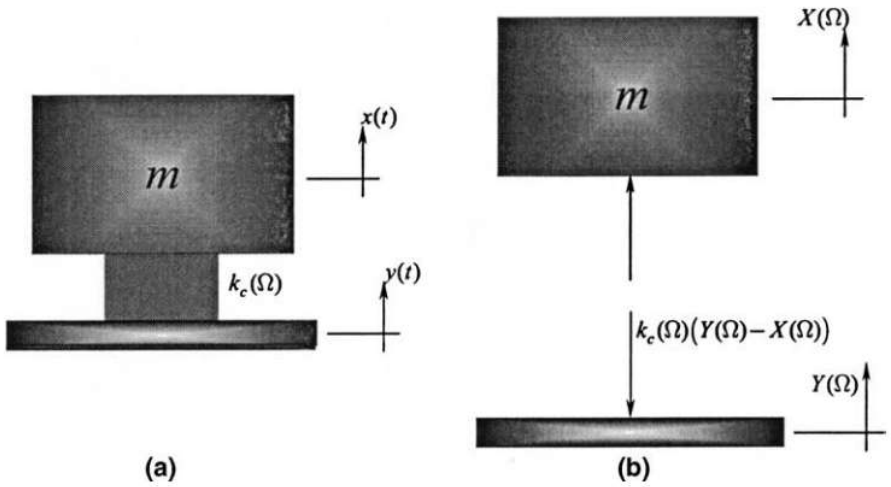

Fig. 2. Transmissibility model for $G_c(\Omega)$ measurement.

The direct complex stiffness method is used to evaluate the viscoelastic material properties.
This model consists of a mass m linked to a rigid basis through a flexible device whose flexibility is provided solely by the viscoelastic part of it. Any inserts or other metallic parts of this device are considered rigid. The movement y(t) of the basis is impressed, or prescribed, and it is assumed not to be affected by any sort of feedback.

$$T_c(\Omega) = \frac{X(\Omega)}{Y(\Omega)} = \frac{k_c(\Omega)}{k_c(\Omega) - m\Omega^2}$$

$$k_c(\Omega) = \vartheta G_c(\Omega)$$

$$T_c(\Omega) = \frac{G_c(\Omega)}{G_c(\Omega) - m_\vartheta \Omega^2}$$

$$m_\vartheta = m/\vartheta.$$

De Espındola, J. J., da Silva Neto, J. M., & Lopes, E. M. (2005). A generalised fractional derivative approach to viscoelastic material properties measurement. Applied Mathematics and Computation, 164(2), 493-506.

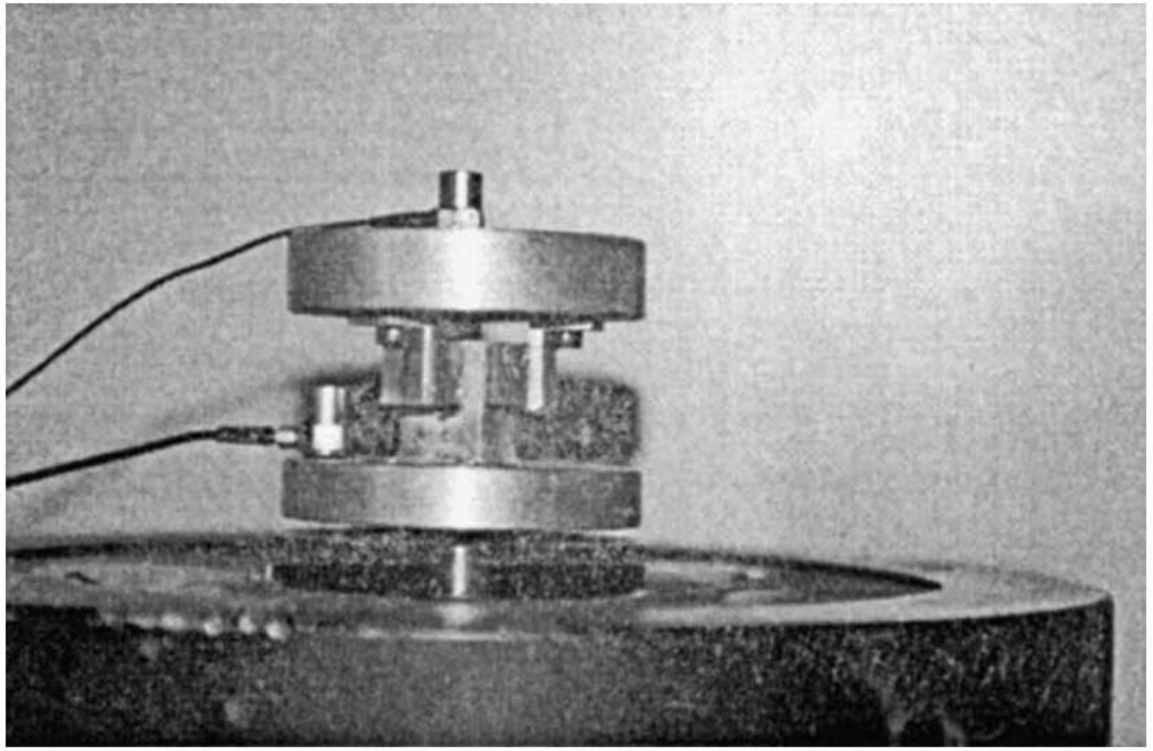

Fig. 3. Photograph of an actual experiment.

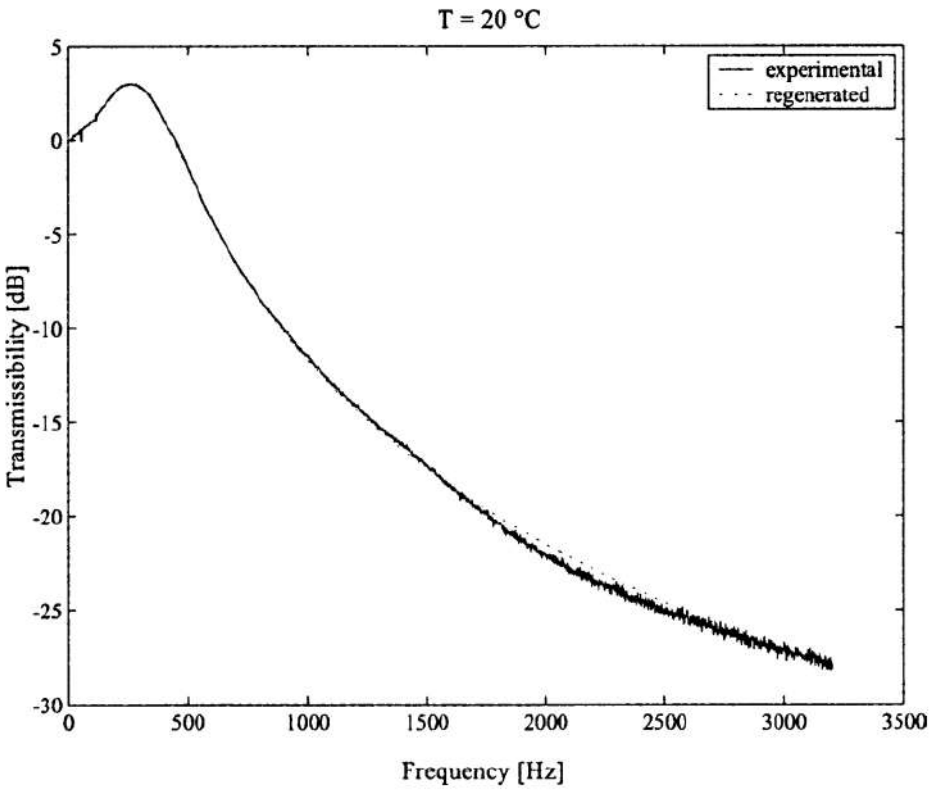

Fig. 4. Transmissibility at 20 °C.

$$\widetilde{T}_c(\Omega_j) = \frac{S_{xy}(\Omega_j)}{S_{yy}(\Omega_j)}, \; j = 1, p,$$

De Espındola, J. J., da Silva Neto, J. M., & Lopes, E. M. (2005). A generalised fractional derivative approach to viscoelastic material properties measurement. Applied Mathematics and Computation, 164(2), 493-506.

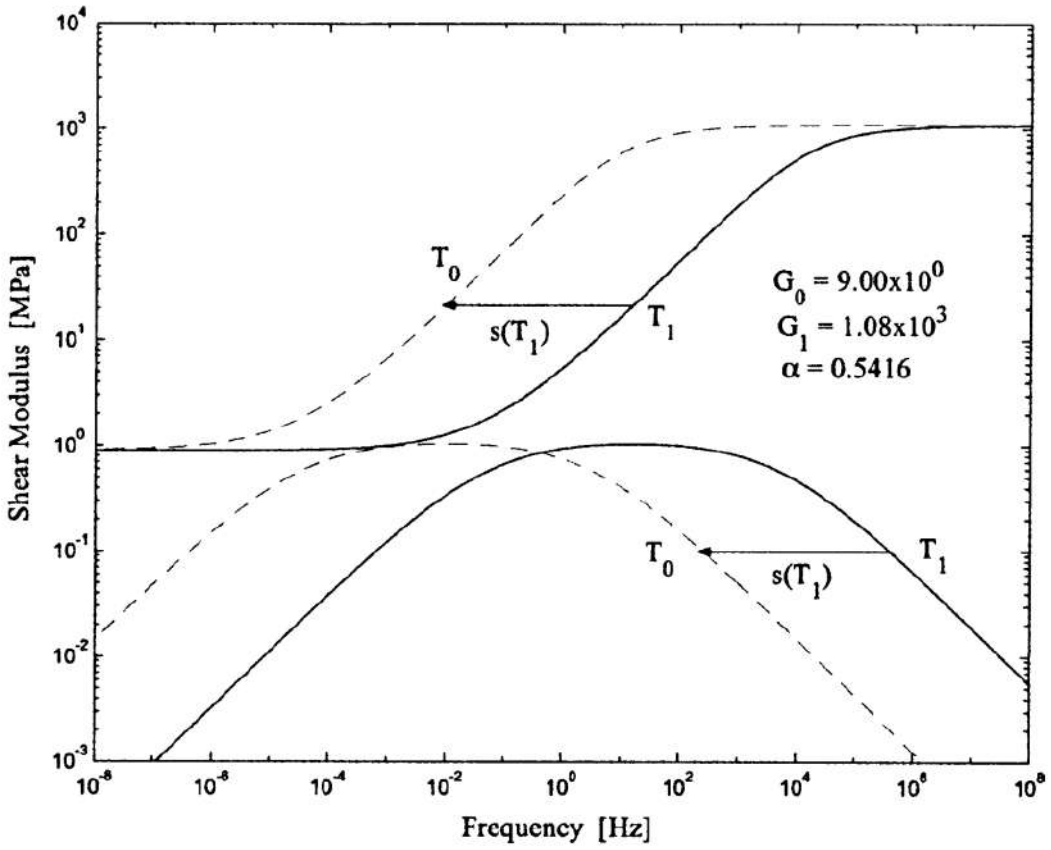

Fig. 7. Behaviour of two curves at T_0 and T_1.

In Figure it is represented how curves for the shear modulus and loss factor, measured at temperatures T0 and T1 and associated with a four parameter model, should appear.

De Espındola, J. J., da Silva Neto, J. M., & Lopes, E. M. (2005). A generalised fractional derivative approach to viscoelastic material properties measurement. Applied Mathematics and Computation, 164(2), 493-506.

Complex modulus approach

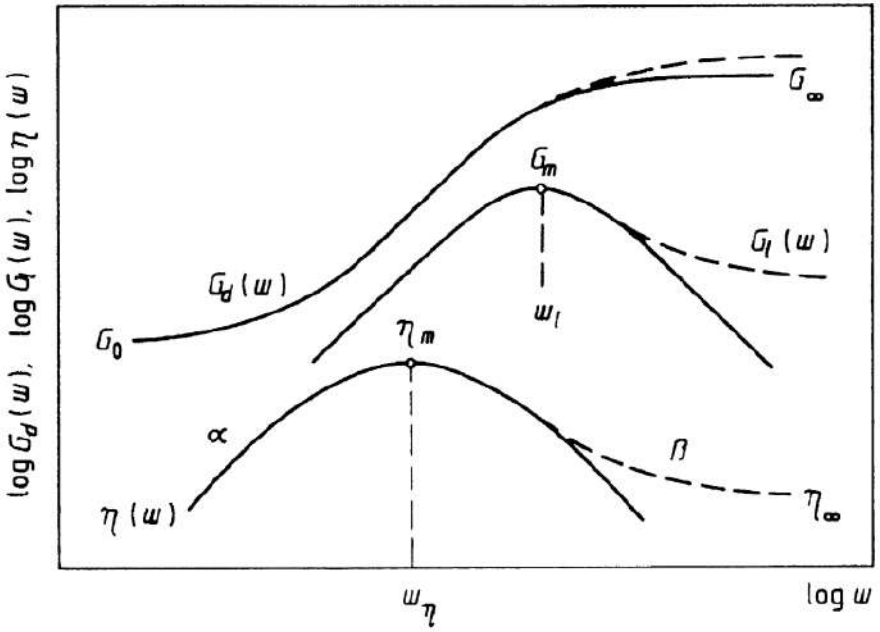

Fig. 1. The experiments made on some polymeric damping materials in a wide frequency range reveal that the loss factor peak is asymmetrical and $\eta(\omega)$ approaches a limit value, while the dynamic modulus exhibits a weak monotonic increase at high frequencies.

$$\bar{G}(\mathrm{j}\omega) = \frac{\tilde{\sigma}(\mathrm{j}\omega)}{\tilde{\varepsilon}(\mathrm{j}\omega)} = G_d(\omega) + \mathrm{j}G_l(\omega) = G_d(\omega)[1 + \mathrm{j}\eta(\omega)]$$

$$\eta(\omega) = \frac{G_l(\omega)}{G_d(\omega)}$$

Pritz, T. (2003). Five-parameter fractional derivative model for polymeric damping materials. Journal of Sound and Vibration, 265(5), 935-952.

The fractional derivative models have been proved to be efficient in describing the dynamic behaviour of real materials, especially polymers used for sound and vibration control. The general form of the constitutive equation for the conventional viscoelastic models is:

$$\sigma(t) + b_1 \frac{\mathrm{d}}{\mathrm{d}t}\sigma(t) + b_2 \frac{\mathrm{d}^2}{\mathrm{d}t^2}\sigma(t) + \cdots + b_n \frac{\mathrm{d}^n}{\mathrm{d}t^n}\sigma(t)$$
$$= a_0\varepsilon(t) + a_1 \frac{\mathrm{d}}{\mathrm{d}t}\varepsilon(t) + a_2 \frac{\mathrm{d}^2}{\mathrm{d}t^2}\varepsilon(t) + \cdots + a_m \frac{\mathrm{d}^m}{\mathrm{d}t^m}\varepsilon(t),$$

It is important to note that the number of time derivatives of stress and strain cannot be arbitrary to insure that the model is physically meaningful satisfying the thermodynamic requirements. The thermodynamic requirements are satisfied only if:

$$m = n \text{ or } m = n + 1$$

Pritz, T. (2003). Five-parameter fractional derivative model for polymeric damping materials. Journal of Sound and Vibration, 265(5), 935-952.

$$\sigma(t) + b_1 \frac{\mathrm{d}^{\beta_1}}{\mathrm{d}t^{\beta_1}} \sigma(t) + b_2 \frac{\mathrm{d}^{\beta_2}}{\mathrm{d}t^{\beta_2}} \sigma(t) + \cdots + b_n \frac{\mathrm{d}^{\beta_n}}{\mathrm{d}t^{\beta_n}} \sigma(t)$$
$$= a_0 \varepsilon(t) + a_1 \frac{\mathrm{d}^{\alpha_1}}{\mathrm{d}t^{\alpha_1}} \varepsilon(t) + a_2 \frac{\mathrm{d}^{\alpha_2}}{\mathrm{d}t^{\alpha_2}} \varepsilon(t) + \cdots + a_m \frac{\mathrm{d}^{\alpha_m}}{\mathrm{d}t^{\alpha_m}} \varepsilon(t),$$

The fractional derivation of the alpha-th order derivative of the strain can be defined by the gamma function:

$$\frac{\mathrm{d}^{\alpha}}{\mathrm{d}t^{\alpha}} \varepsilon(t) = \frac{1}{\Gamma(1-\alpha)} \frac{\mathrm{d}}{\mathrm{d}t} \int_0^t \frac{\varepsilon(\tau)}{(t-\tau)^{\alpha}} \mathrm{d}\tau.$$

Among the models, the fractional Zener model has been found to be efficient to predict the symmetrical loss factor peak behavior. The constitutive equation for this model can be derived as follows:

$$\sigma(t) + b_1 \frac{\mathrm{d}^{\beta_1}}{\mathrm{d}t^{\beta_1}} \sigma(t) = a_0 \varepsilon(t) + a_1 \frac{\mathrm{d}^{\alpha_1}}{\mathrm{d}t^{\alpha_1}} \varepsilon(t).$$

$$b_1 = \tau^{\alpha},$$

$$a_0 = G_0,$$

$$a_1 = G_{\infty} \tau^{\alpha},$$

Pritz, T. (2003). Five-parameter fractional derivative model for polymeric damping materials. Journal of Sound and Vibration, 265(5), 935-952.

$$\sigma(t) + \tau^{\alpha} \frac{\mathrm{d}^{\alpha}}{\mathrm{d}t^{\alpha}} \sigma(t) = G_0 \varepsilon(t) + G_{\infty} \tau^{\alpha} \frac{\mathrm{d}^{\alpha}}{\mathrm{d}t^{\alpha}} \varepsilon(t).$$

$$F \frac{\mathrm{d}^{\alpha}}{\mathrm{d}t^{\alpha}} \varepsilon(t) = (\mathrm{j}\omega)^{\alpha} F \varepsilon(t),$$

The complex modulus of the model can be derived by transforming the time domain equation into the frequency domain:

$$\bar{G}(\mathrm{j}\omega) = G_0 \frac{1 + d(\mathrm{j}\omega\tau)^{\alpha}}{1 + (\mathrm{j}\omega\tau)^{\alpha}},$$

$$d = \frac{G_{\infty}}{G_0}.$$

Pritz, T. (2003). Five-parameter fractional derivative model for polymeric damping materials. Journal of Sound and Vibration, 265(5), 935-952.

$$\bar{G}(j\omega) = G_0 + G_0(d-1)\frac{(j\omega\tau)^{\alpha}}{1+(j\omega\tau)^{\alpha}}.$$

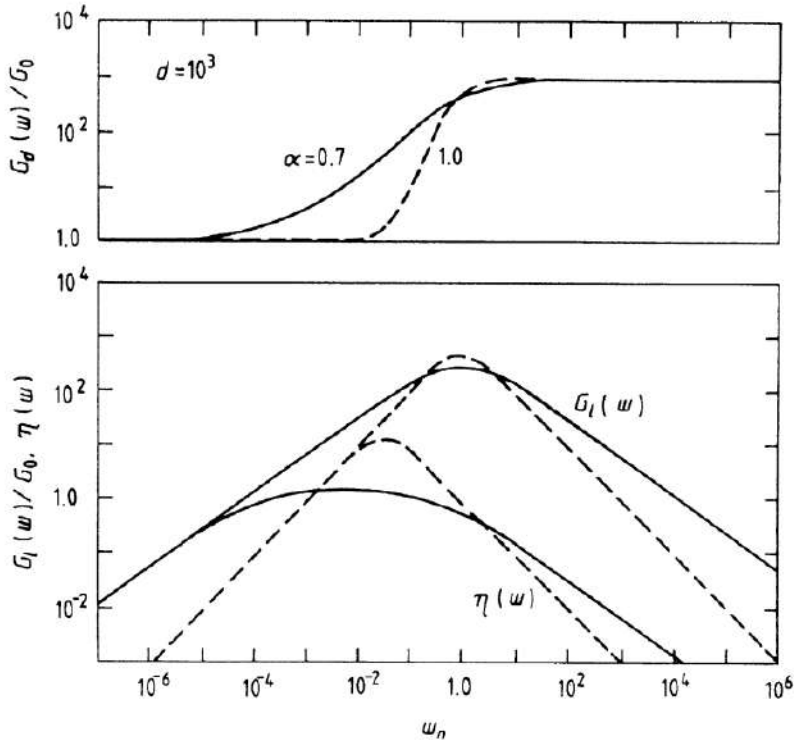

Fig. 2. Frequency variations of the dynamic modulus, loss modulus and loss factor predicted by the four-parameter fractional Zener model (—) and the conventional Zener model (- - - -), respectively.

The four-parameter fractional Zener model has solid theoretical basis, it is related to the general fractional derivative constitutive equation of viscoelastic materials as discussed above, moreover the model is causal and satisfies the thermodynamic constraints. The model has successfully been fitted to experimental data on a wide variety of materials, especially polymers for vibration damping. Nevertheless, the four-parameter model is not able to predict asymmetrical loss peak.

Pritz, T. (2003). Five-parameter fractional derivative model for polymeric damping materials. Journal of Sound and Vibration, 265(5), 935-952.

The number of time derivatives of strain is reasonable to increase in order to improve the viscoelastic model and to reproduce asymmetrical loss peak behavior:

$$\sigma(t) + b_1 \frac{\mathrm{d}^{\beta_1}}{\mathrm{d}t^{\beta_1}} \sigma(t) = a_0 \varepsilon(t) + a_1 \frac{\mathrm{d}^{\alpha_1}}{\mathrm{d}t^{\alpha_1}} \varepsilon(t) + a_2 \frac{\mathrm{d}^{\alpha_2}}{\mathrm{d}t^{\alpha_2}} \varepsilon(t),$$

$$b_1 = \tau^{\beta},$$

$$a_0 = G_0,$$

$$a_1 = G_1 \tau^{\beta},$$

$$a_2 = G_2 \tau^{\alpha},$$

Pritz, T. (2003). Five-parameter fractional derivative model for polymeric damping materials. Journal of Sound and Vibration, 265(5), 935-952.

$$\sigma(t) + \tau^{\beta} \frac{\mathrm{d}^{\beta}}{\mathrm{d}t^{\beta}} \sigma(t) = G_0 \varepsilon(t) + G_1 \tau^{\beta} \frac{\mathrm{d}^{\beta}}{\mathrm{d}t^{\beta}} \varepsilon(t) + G_2 \tau^{\alpha} \frac{\mathrm{d}^{\alpha}}{\mathrm{d}t^{\alpha}} \varepsilon(t),$$

Reducing the number of independent constants:

$$G_1 = G_0$$

$$G_2 = G_{\infty} - G_0.$$

$$\sigma(t) + \tau^{\beta} \frac{\mathrm{d}^{\beta}}{\mathrm{d}t^{\beta}} \sigma(t) = G_0 \varepsilon(t) + G_0 \tau^{\beta} \frac{\mathrm{d}^{\beta}}{\mathrm{d}t^{\beta}} \varepsilon(t) + (G_{\infty} - G_0) \tau^{\alpha} \frac{\mathrm{d}^{\alpha}}{\mathrm{d}t^{\alpha}} \varepsilon(t).$$

Pritz, T. (2003). Five-parameter fractional derivative model for polymeric damping materials. Journal of Sound and Vibration, 265(5), 935-952.

$$\bar{G}(j\omega) = G_0 + G_0(d-1)\frac{(j\omega\tau)^{\alpha}}{1+(j\omega\tau)^{\beta}}.$$

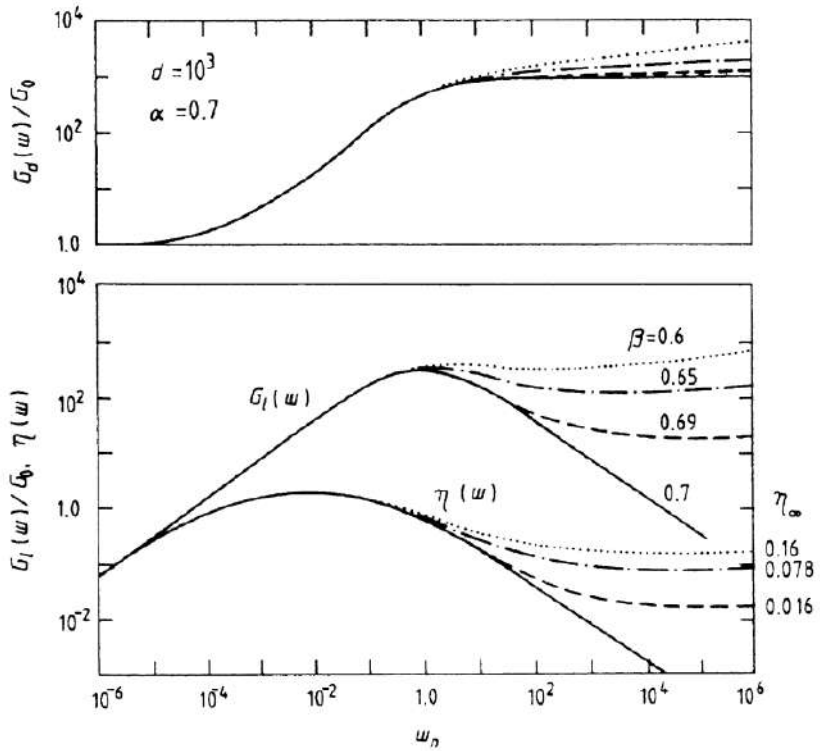

Fig. 3. Frequency variations of dynamic modulus, loss modulus and loss factor predicted by the five-parameter fractional Zener model (----, —· –, ···) and the four-parameter fractional Zener model (—), respectively.

In Figure it is demonstrated that there is a striking difference between the behaviours of the five- and the four- parameter models at high frequencies. Nevertheless, the low-frequency behaviour of these models is practically the same.

Pritz, T. (2003). Five-parameter fractional derivative model for polymeric damping materials. Journal of Sound and Vibration, 265(5), 935-952.

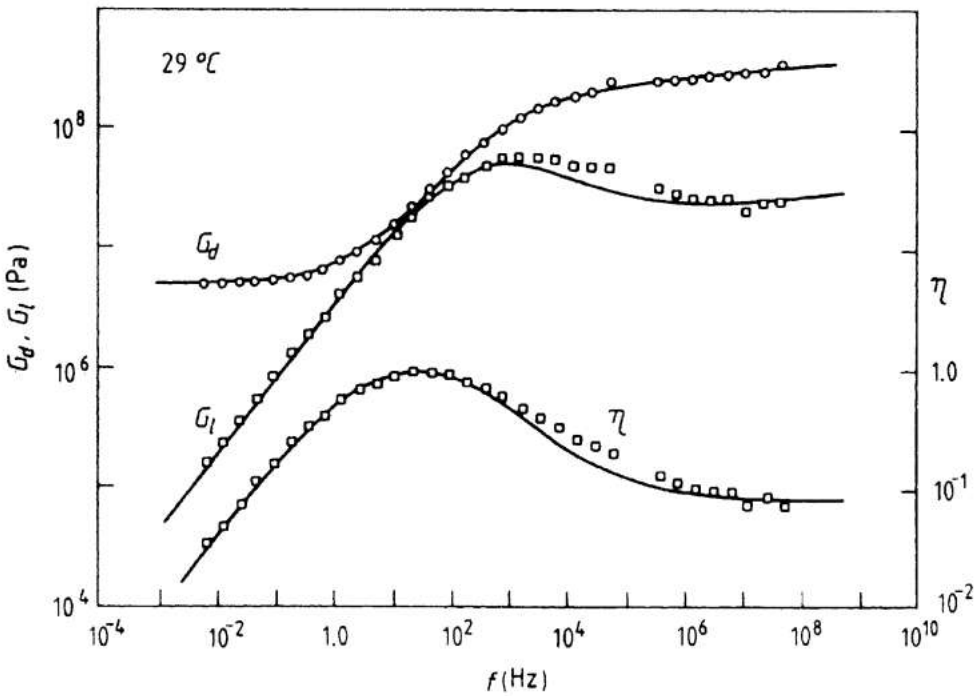

Fig. 5. Dynamic shear properties of damping material GE.SMRD. □, ○, Experimental data from Ref. [6] (some overlapping data have been omitted for the sake of clarity); —, calculated by the five-parameter fractional Zener model with the parameters given in Table 1.

Pritz, T. (2003). Five-parameter fractional derivative model for polymeric damping materials. Journal of Sound and Vibration, 265(5), 935-952.

Table 1
Parameter values determined for the five-parameter fractional Zener model

Material	G_0 (Pa)	G_∞ (Pa)	d	η_∞	α	β	f_l (Hz)	τ (s)
GE.SMRD	5×10^6	1.8×10^8	36	0.08	0.605	0.554	760	2.09×10^{-4}
EAR C-1002	8×10^5	1.256×10^9	1570	0.012	0.566	0.558	2.2×10^6	7.23×10^{-10}

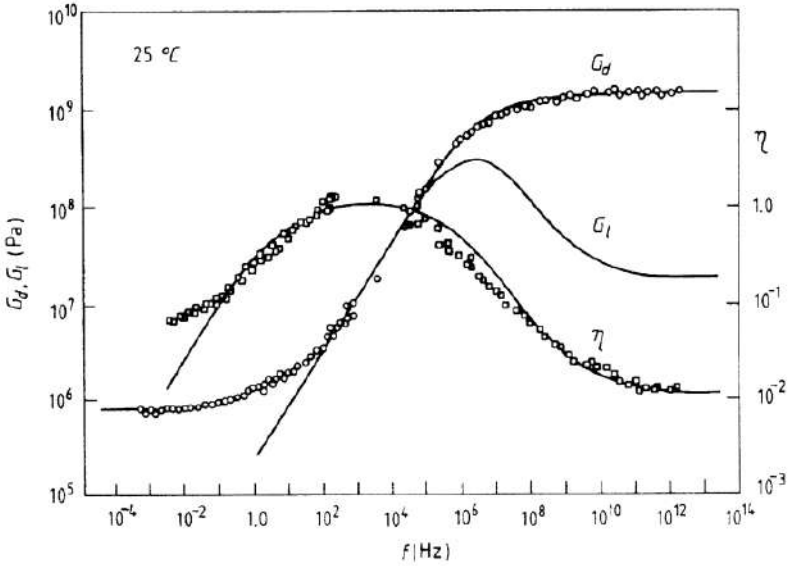

Fig. 6. Dynamic shear properties of damping material EAR C-1002. □, ○, Experimental data from Ref. [7] (some overlapping and erroneous data have been omitted for the sake of clarity); —, calculated by the five-parameter fractional Zener model with the parameters given in Table 1.

Pritz, T. (2003). Five-parameter fractional derivative model for polymeric damping materials. Journal of Sound and Vibration, 265(5), 935-952.

Viscoelastic multilayered panels frequency-response analysis

The frequency-response analysis of a viscoleastic multilayered panel structure is performed by the use of the Principle of Virtual Displacements (**PVD**).

$$\int_{\Omega}\int_{A} \delta\varepsilon^T \boldsymbol{\sigma}\, d\Omega dz + \int_{\Omega}\int_{A} \rho\, \delta\boldsymbol{u}^T \ddot{\boldsymbol{u}}\, d\Omega dz = \int_{\Omega}\int_{A} \delta\boldsymbol{u}^T \bar{t}\, d\Omega dz$$

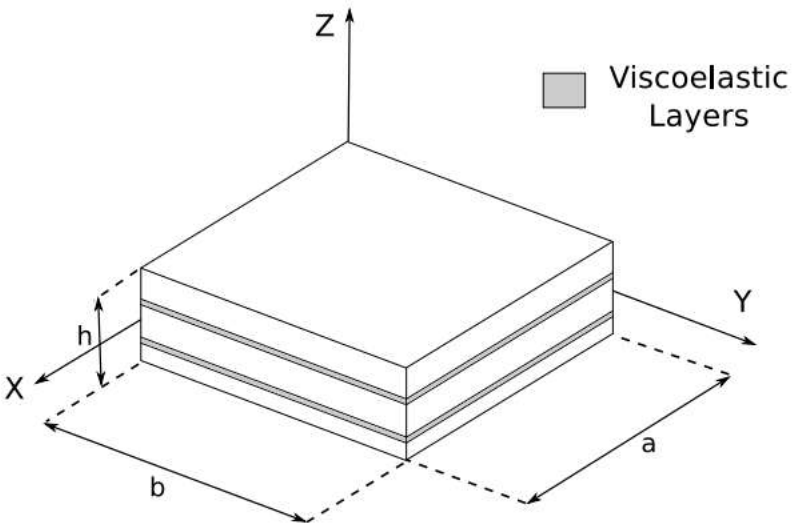

Fig. 1. Geometry and reference system of the multilayered plate, including viscoelastic layers.

The governing equations can be derived in compact form:

$$(\boldsymbol{K}(\omega) - \omega^2 \boldsymbol{M})\boldsymbol{u} = \boldsymbol{P}_0$$

Filippi, M., Carrera, E., & Valvano, S. (2018). Analysis of multilayered structures embedding viscoelastic layers by higher-order, and zig-zag plate elements. Composites Part B: Engineering, 154, 77-89.

Different kinematic approaches

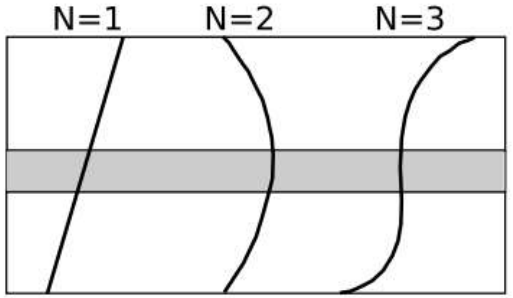

Fig. 2. Higher-Order behaviour of the primary variables along the thickness of the plate.

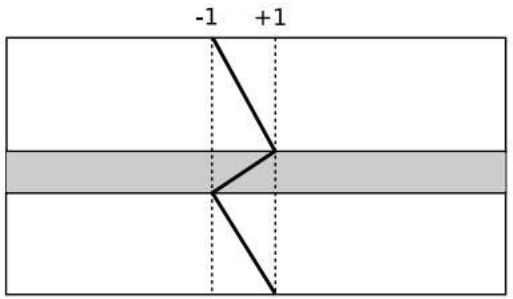

Fig. 3. Murakami zig-zag function along the thickness of the plate.

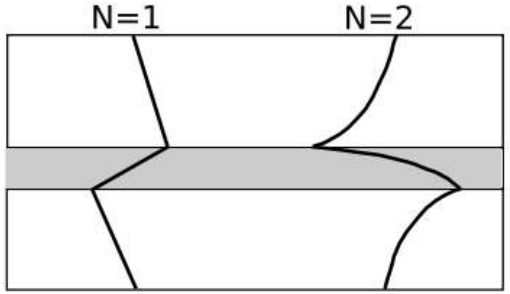

Fig. 5. Layer-Wise behaviour of the primary variables along the thickness of the plate.

Filippi, M., Carrera, E., & Valvano, S. (2018). Analysis of multilayered structures embedding viscoelastic layers by higher-order, and zig-zag plate elements. Composites Part B: Engineering, 154, 77-89.

Composite sandwich plate with viscoelastic core

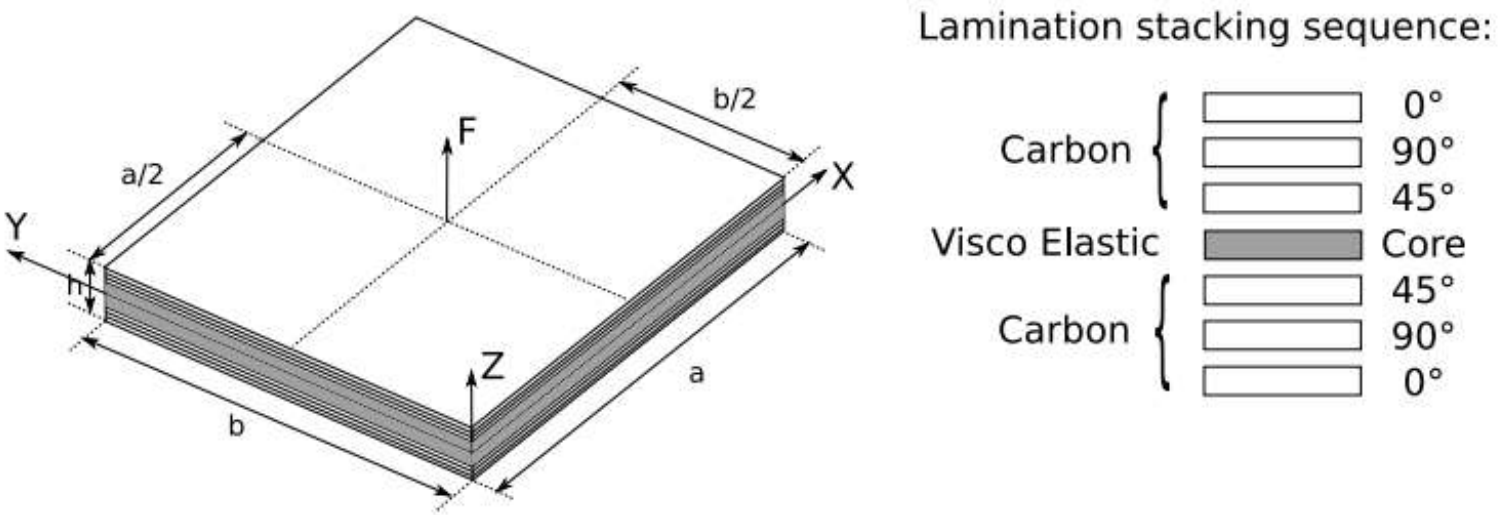

Fig. 16. Geometry and reference system of the multilayered plate, and its relative lamination stacking sequence.

Filippi, M., Carrera, E., & Valvano, S. (2018). Analysis of multilayered structures embedding viscoelastic layers by higher-order, and zig-zag plate elements. Composites Part B: Engineering, 154, 77-89.

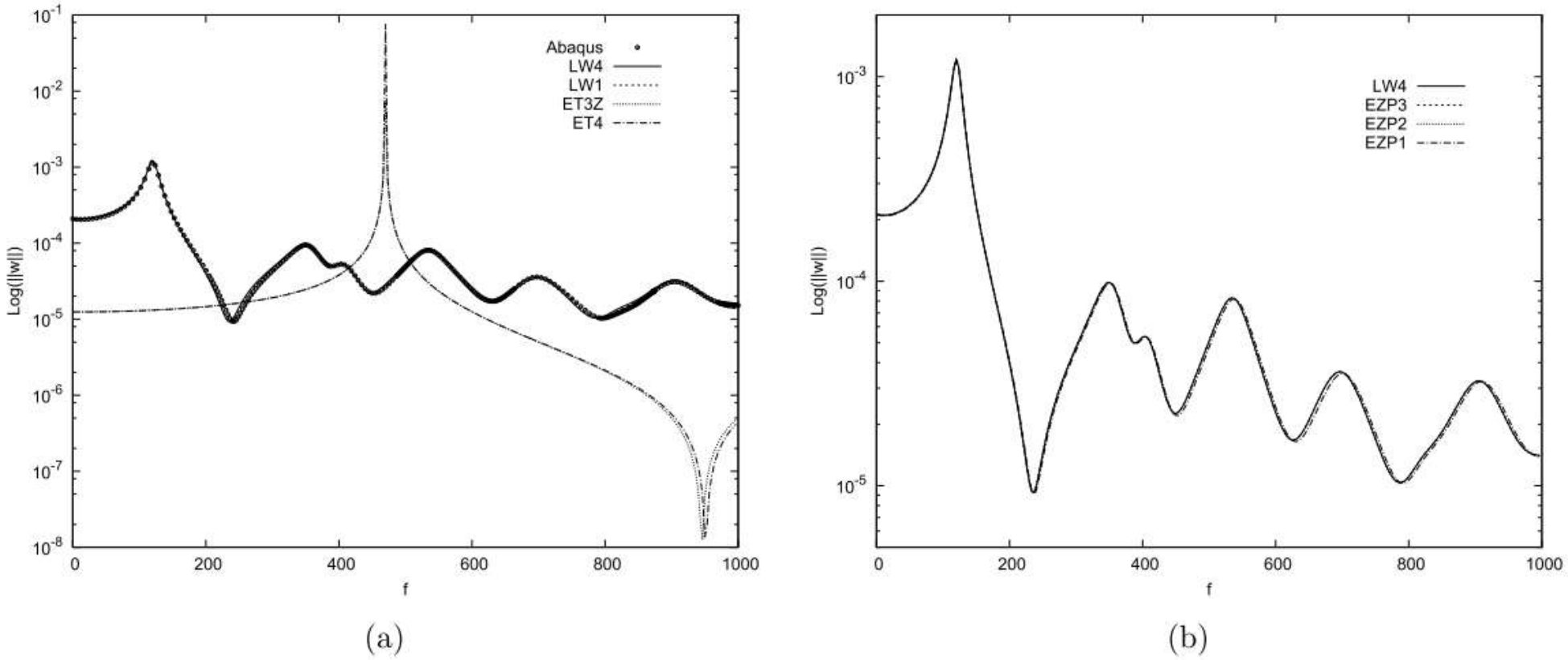

Fig. 17. Seven-layered plate with frequency-dependent damping viscoelastic core. Frequency response of the transverse displacement magnitude $||w||(x, y, z) = ||w||(a/2, b/2, +h/2)$ for different theories.

Filippi, M., Carrera, E., & Valvano, S. (2018). Analysis of multilayered structures embedding viscoelastic layers by higher-order, and zig-zag plate elements. Composites Part B: Engineering, 154, 77-89.

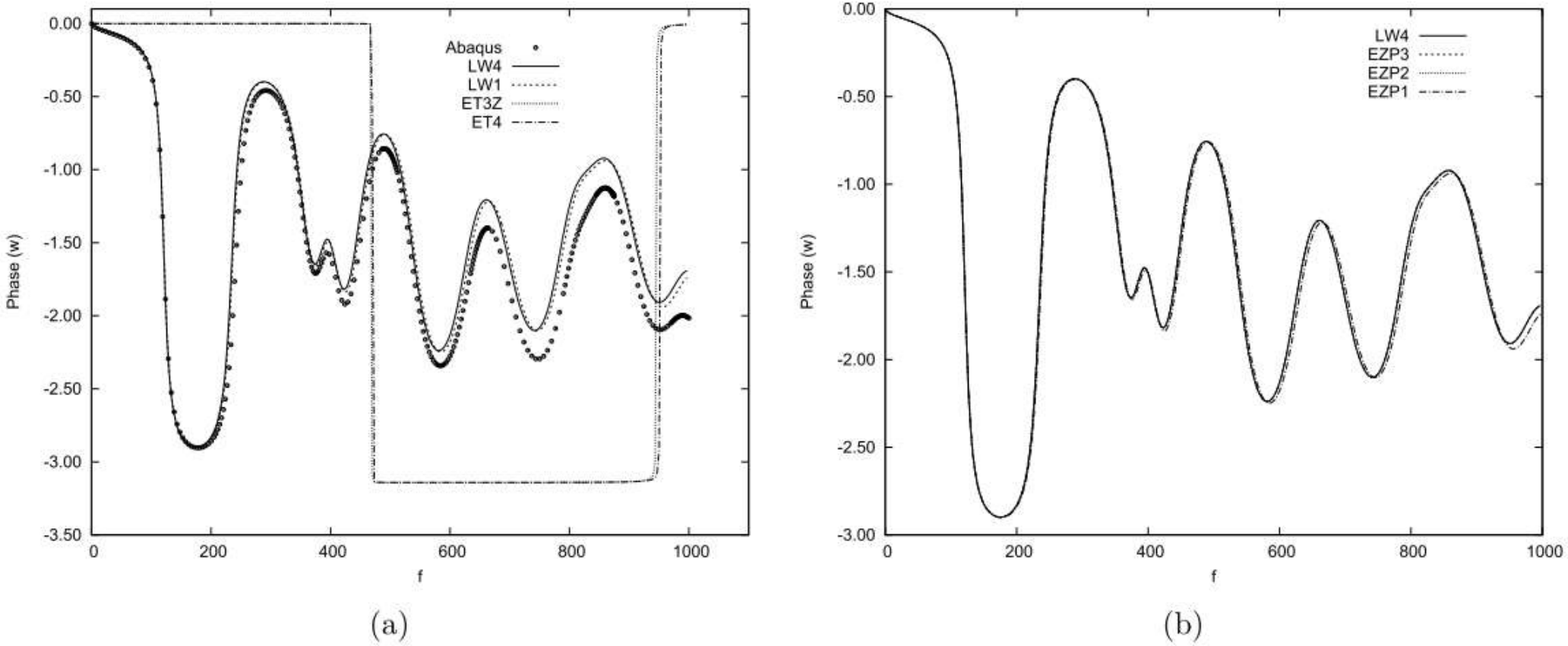

Fig. 18. Seven-layered plate with frequency-dependent damping viscoelastic core. Frequency response of the transverse displacement phase, $Phase(w)(x, y, z) = Phase(w)(a/2, b/2, +h/2)$ for different theories.

Filippi, M., Carrera, E., & Valvano, S. (2018). Analysis of multilayered structures embedding viscoelastic layers by higher-order, and zig-zag plate elements. Composites Part B: Engineering, 154, 77-89.

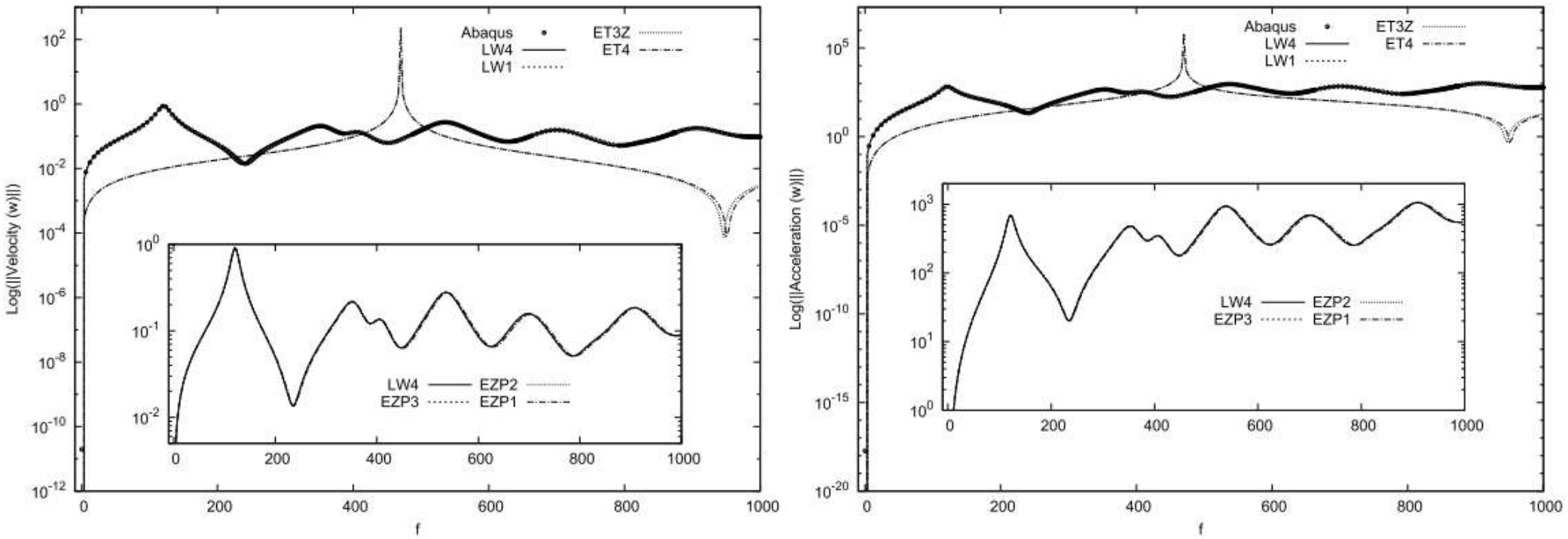

(a) $||Velocity(w)||$ (b) $||Acceleration(w)||$

Fig. 19. Seven-layered plate with frequency-dependent damping viscoelastic core. Frequency response of the velocity and acceleration magnitude related to the transverse displacement $||v(w)||(x, y, z) = ||v(w)||(a/2, b/2, +h/2)$, $||a(w)||(x, y, z) = ||a(w)||(a/2, b/2, +h/2)$ for different theories.

Filippi, M., Carrera, E., & Valvano, S. (2018). Analysis of multilayered structures embedding viscoelastic layers by higher-order, and zig-zag plate elements. Composites Part B: Engineering, 154, 77-89.

Lattice cell structure for aeronautical sandwich panels

Composite lattice applications

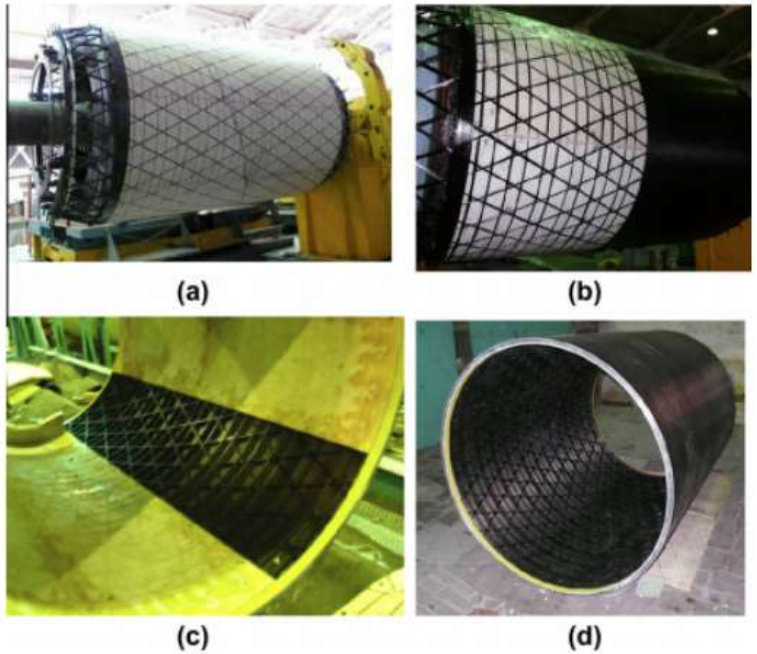

Figura 2.6: Produzione di strutture composite lattice

Figura 2.10: Adattatore di carico utile metallico ed in composito a griglia

Verholle, K. (2021). ANALISI STATICA E VIBRAZIONI LIBERE PER PANNELLI SANDWICH CON CUORE REALIZZATO MEDIANTE STRUTTURE LATTICE= STATIC ANALYSIS AND FREE VIBRATIONS FOR SANDWICH PANELS WITH CORE MADE BY LATTICE STRUCTURES (Doctoral dissertation, Ph. D. Thesis, Politecnico di Torino, Turin, Italy).

Filament winding technique

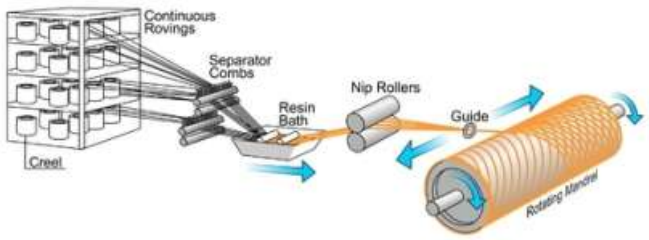

Figura 2.4: Schema processo filament winding

Figura 2.5: Esempio di componente ottenuto con filament winding

Verholle, K. (2021). ANALISI STATICA E VIBRAZIONI LIBERE PER PANNELLI SANDWICH CON CUORE REALIZZATO MEDIANTE STRUTTURE LATTICE= STATIC ANALYSIS AND FREE VIBRATIONS FOR SANDWICH PANELS WITH CORE MADE BY LATTICE STRUCTURES (Doctoral dissertation, Ph. D. Thesis, Politecnico di Torino, Turin, Italy).

Aerospace structures lattice applications

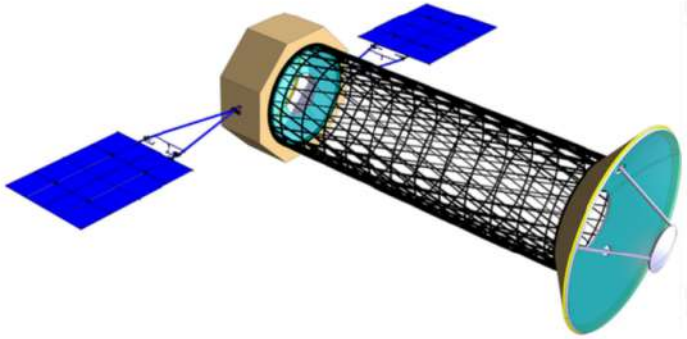

Figura 2.12: Struttura composita reticolare di un satellite

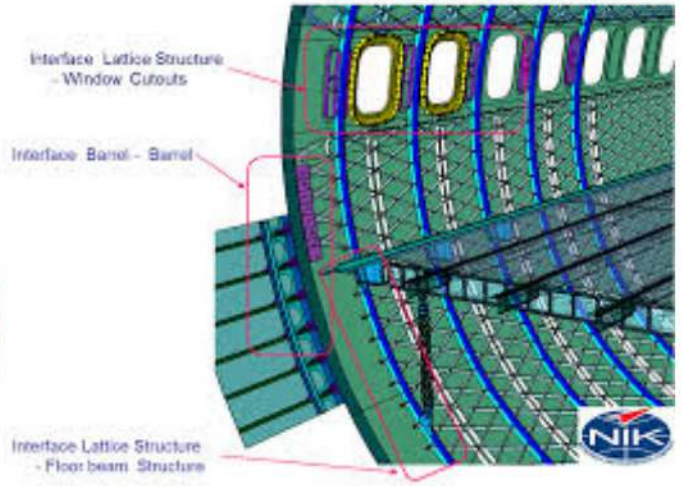

Figura 2.13: Fusoliera aerea con struttura lattice

Verholle, K. (2021). ANALISI STATICA E VIBRAZIONI LIBERE PER PANNELLI SANDWICH CON CUORE REALIZZATO MEDIANTE STRUTTURE LATTICE= STATIC ANALYSIS AND FREE VIBRATIONS FOR SANDWICH PANELS WITH CORE MADE BY LATTICE STRUCTURES (Doctoral dissertation, Ph. D. Thesis, Politecnico di Torino, Turin, Italy).

Composite lattice shell

Figura 2.3: Esempio di struttura lattice di un guscio cilindrico

Verholle, K. (2021). ANALISI STATICA E VIBRAZIONI LIBERE PER PANNELLI SANDWICH CON CUORE REALIZZATO MEDIANTE STRUTTURE LATTICE= STATIC ANALYSIS AND FREE VIBRATIONS FOR SANDWICH PANELS WITH CORE MADE BY LATTICE STRUCTURES (Doctoral dissertation, Ph. D. Thesis, Politecnico di Torino, Turin, Italy).

Lattice wing concept

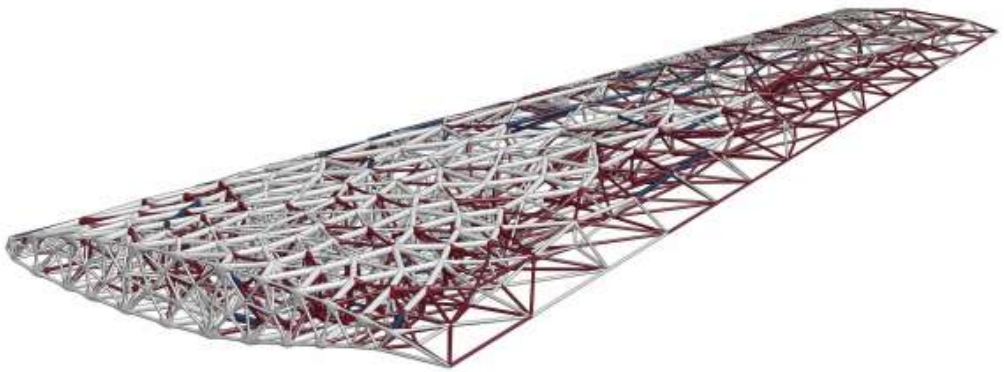

Figura 2.14: Concept di ala con struttura lattice a forma variabile

Verholle, K. (2021). ANALISI STATICA E VIBRAZIONI LIBERE PER PANNELLI SANDWICH CON CUORE REALIZZATO MEDIANTE STRUTTURE LATTICE= STATIC ANALYSIS AND FREE VIBRATIONS FOR SANDWICH PANELS WITH CORE MADE BY LATTICE STRUCTURES (Doctoral dissertation, Ph. D. Thesis, Politecnico di Torino, Turin, Italy).

Sandwich panel with honeycomb core

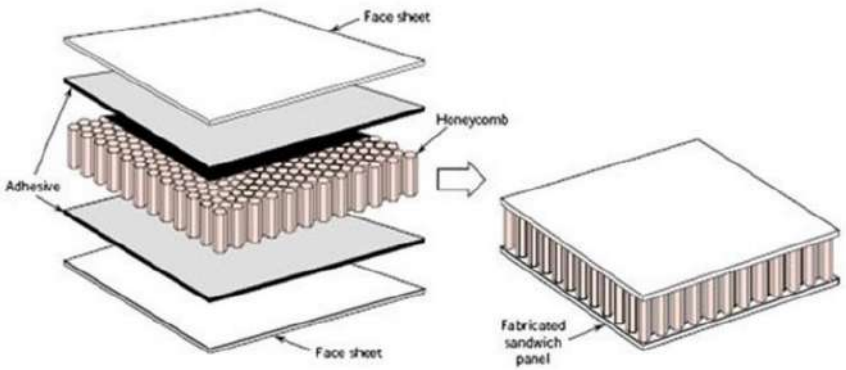

Figura 2.1: Pannello sandwich con cuore a nido d’ape

Verholle, K. (2021). ANALISI STATICA E VIBRAZIONI LIBERE PER PANNELLI SANDWICH CON CUORE REALIZZATO MEDIANTE STRUTTURE LATTICE= STATIC ANALYSIS AND FREE VIBRATIONS FOR SANDWICH PANELS WITH CORE MADE BY LATTICE STRUCTURES (Doctoral dissertation, Ph. D. Thesis, Politecnico di Torino, Turin, Italy).

Lattice cell structures obtained with Selective Laser Melting process

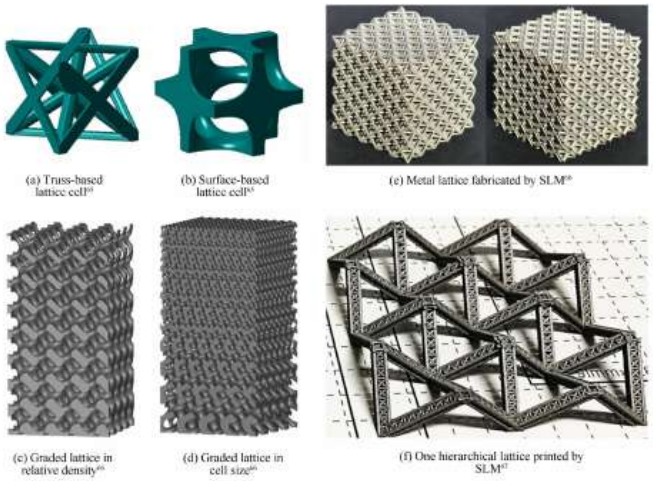

Figura 2.8: Campioni realizzati con SLM

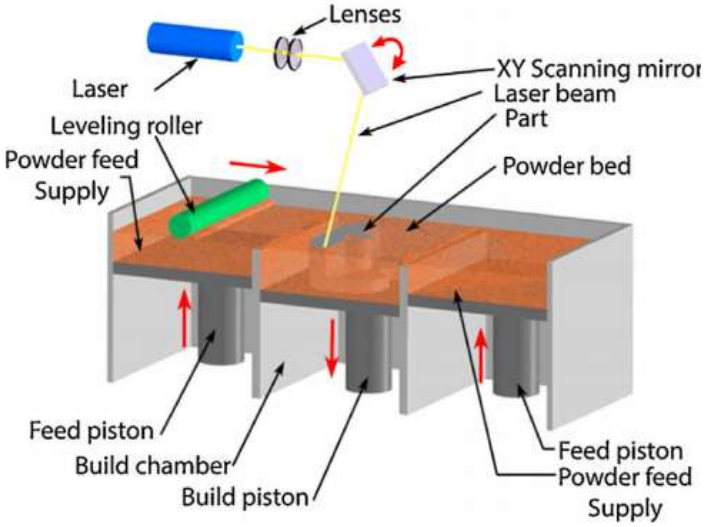

Figura 2.9: Processo di SLM

Verholle, K. (2021). ANALISI STATICA E VIBRAZIONI LIBERE PER PANNELLI SANDWICH CON CUORE REALIZZATO MEDIANTE STRUTTURE LATTICE= STATIC ANALYSIS AND FREE VIBRATIONS FOR SANDWICH PANELS WITH CORE MADE BY LATTICE STRUCTURES (Doctoral dissertation, Ph. D. Thesis, Politecnico di Torino, Turin, Italy).

Sandwich panels with different lattice core structures

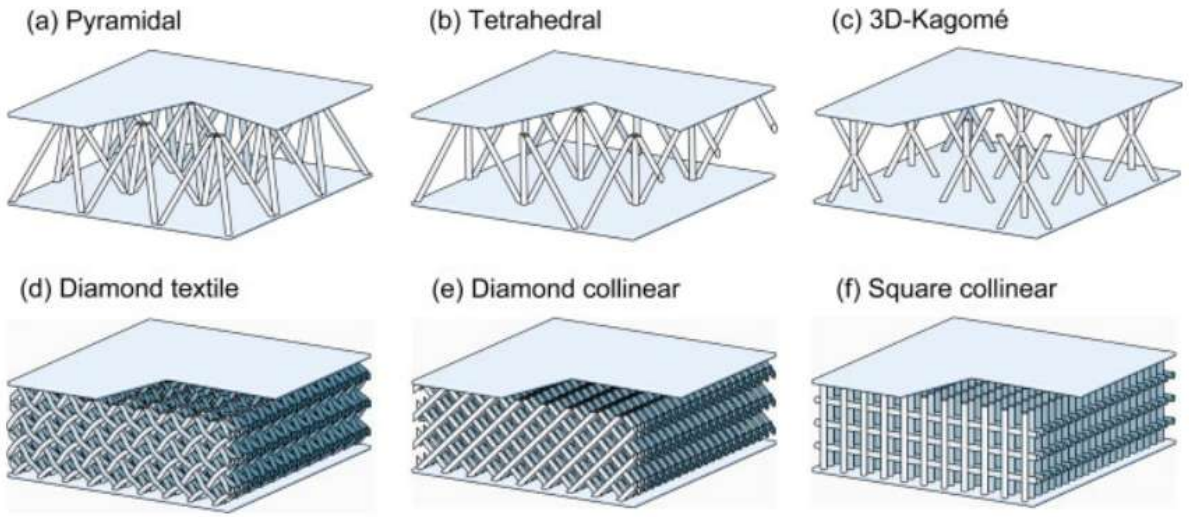

Figura 2.2: Diverse tipologie di pannelli sandwich con cuore in struttura lattice

Verholle, K. (2021). ANALISI STATICA E VIBRAZIONI LIBERE PER PANNELLI SANDWICH CON CUORE REALIZZATO MEDIANTE STRUTTURE LATTICE= STATIC ANALYSIS AND FREE VIBRATIONS FOR SANDWICH PANELS WITH CORE MADE BY LATTICE STRUCTURES (Doctoral dissertation, Ph. D. Thesis, Politecnico di Torino, Turin, Italy).

Sandwich lattice panel application

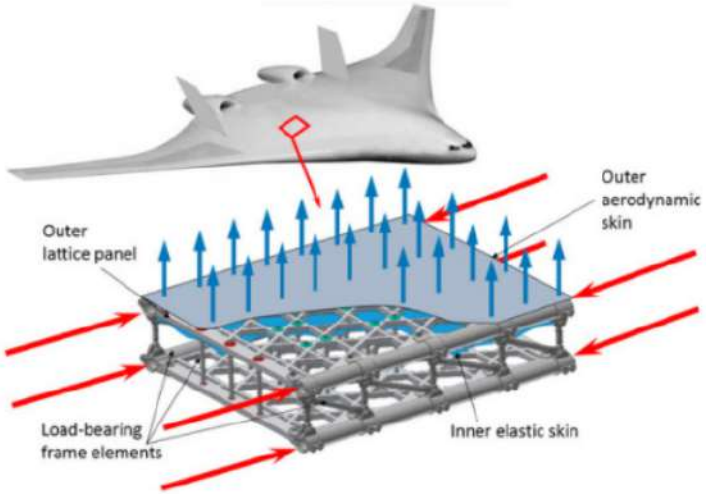

Figura 2.15: Concept di velivolo con pannelli in struttura lattice

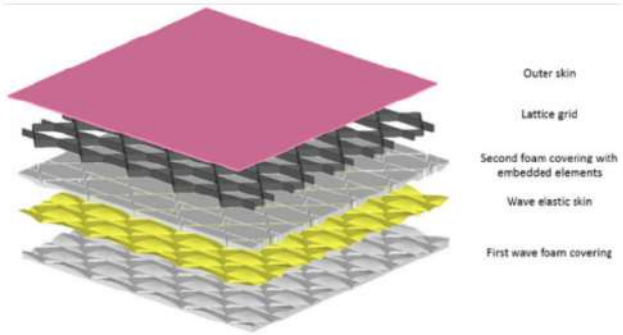

Figura 2.16: Composizione di un pannello innovativo in struttura lattice

Verholle, K. (2021). ANALISI STATICA E VIBRAZIONI LIBERE PER PANNELLI SANDWICH CON CUORE REALIZZATO MEDIANTE STRUTTURE LATTICE= STATIC ANALYSIS AND FREE VIBRATIONS FOR SANDWICH PANELS WITH CORE MADE BY LATTICE STRUCTURES (Doctoral dissertation, Ph. D. Thesis, Politecnico di Torino, Turin, Italy).

Lattice cell examples

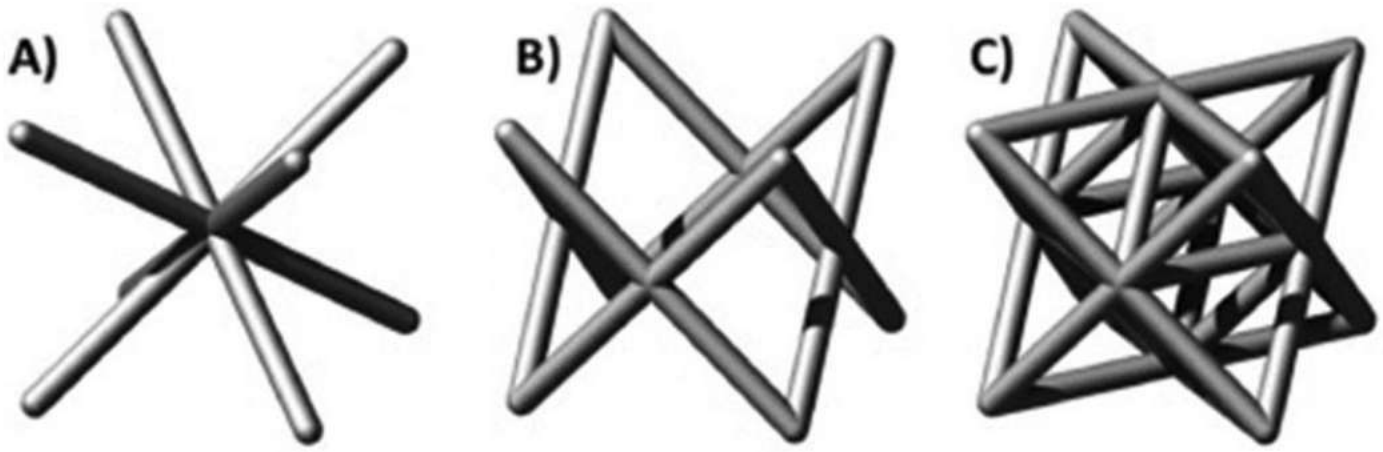

Fig. 1. Geometry of typical lattice cells: BCC (A), FCC (B) Octet (C).

Davide Tumino, Andrea Alaimo, Calogero Orlando, Stefano Valvano (2021). A preliminary Study on the Effect of Strut Waviness on the mechanical Properties of BCC Lattice unit Cells. ADM 2021 International Conference Design Tools and Methods in Industrial Engineering, 9th-10th September – Sapienza University of Rome (Italy).

For 2-D lattice, very recent attempts have been done to introduce waviness in stretch and in bending dominated cells in order to modify the equivalent elastic response of each lattice. **An enhanced ductility has been obtained for different geometries for a fixed valued of the relative density equal to 0.1.**

Triangular

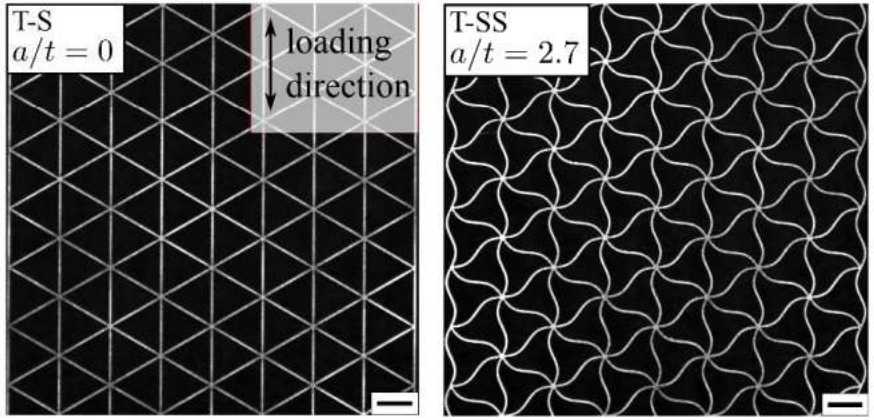

Straight side Waved side

Hexagonal

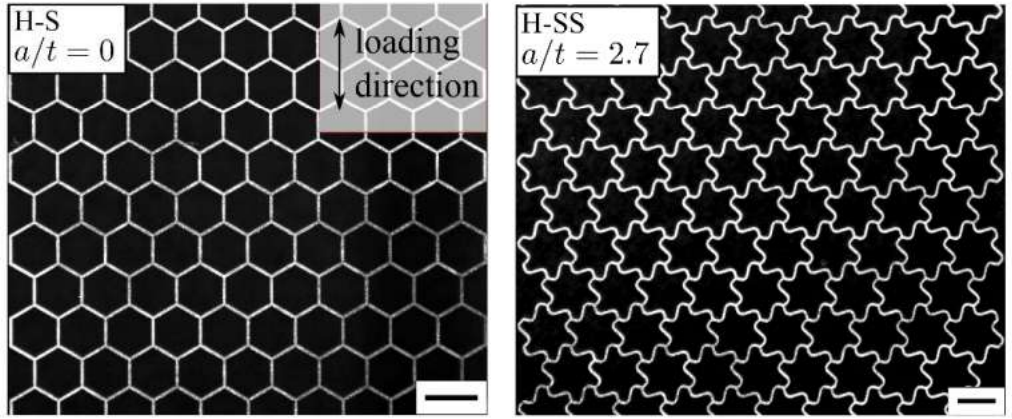

Straight side Waved side

Seiler, P.E., Li, K., Deshpande, V.S., Fleck, N.A. (2021) Journal of Applied Mechanics, Transactions ASME, 88 (3)

Davide Tumino, Andrea Alaimo, Calogero Orlando, Stefano Valvano (2021). A preliminary Study on the Effect of Strut Waviness on the mechanical Properties of BCC Lattice unit Cells. ADM 2021 International Conference Design Tools and Methods in Industrial Engineering, 9th-10th September – Sapienza University of Rome (Italy).

Homogenized material

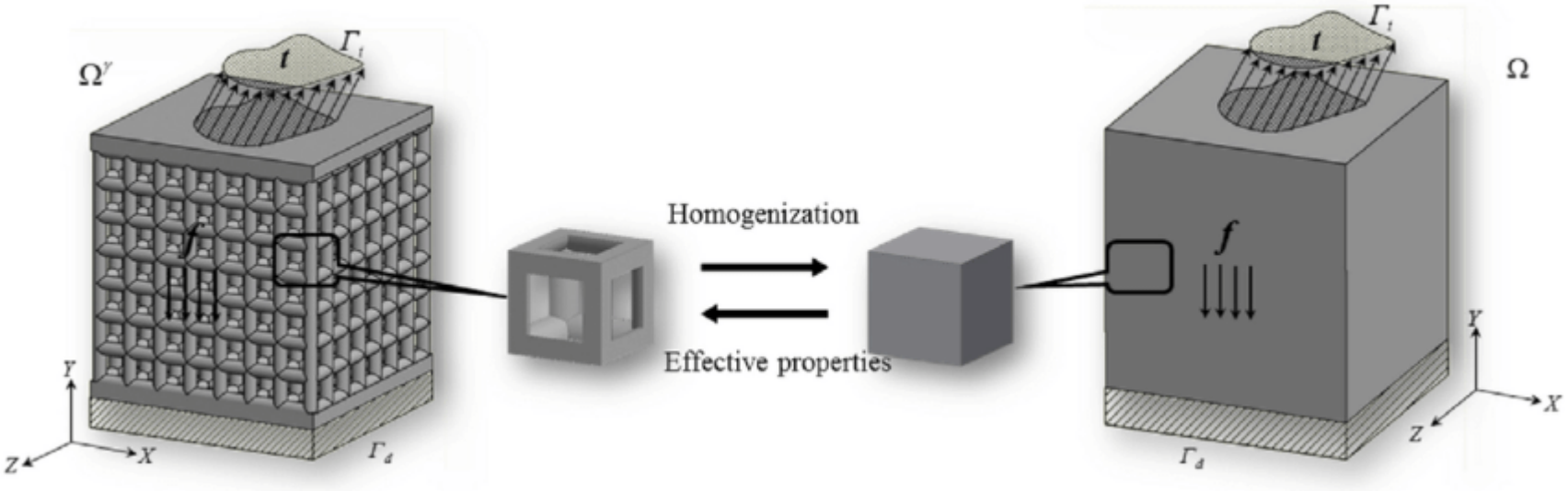

Cheng, L., Liang, X., Belski, E., Wang, X., Sietins, J. M., Ludwick, S., & To, A. (2018). Natural frequency optimization of variable-density additive manufactured lattice structure: theory and experimental validation. Journal of Manufacturing Science and Engineering, 140(10).

Struts waviness concept

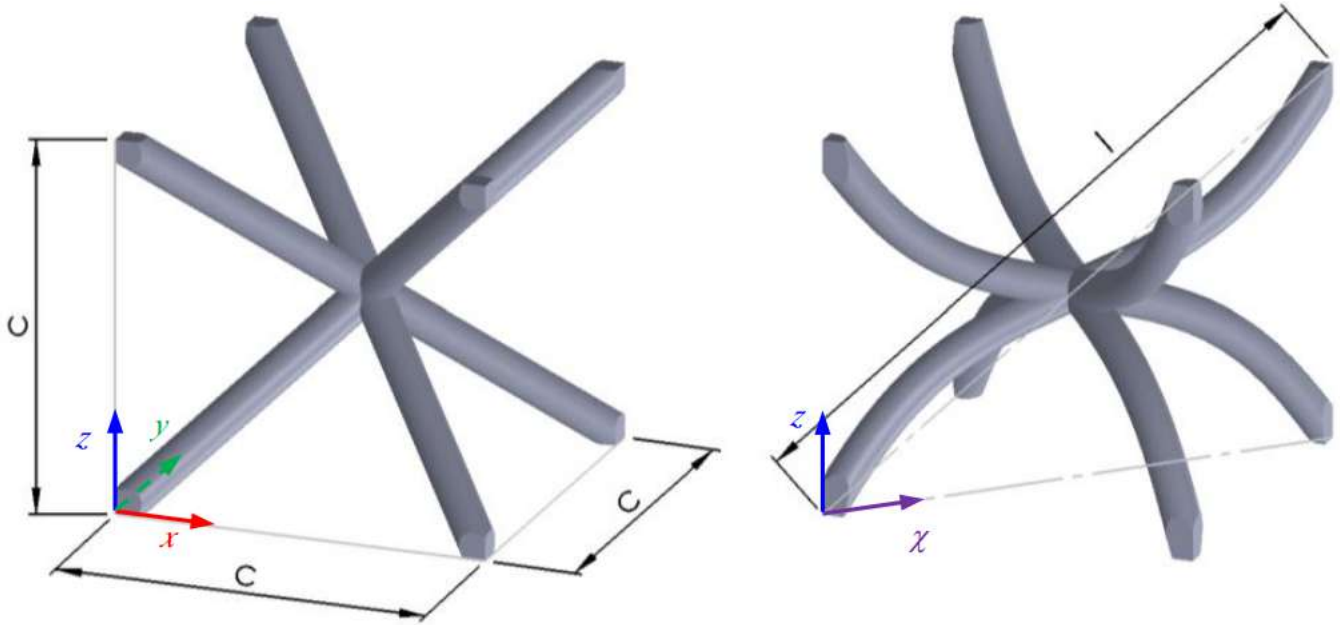

Fig. 2. Geometry of the BCC models: straight strut (left) and waved strut (right).

Davide Tumino, Andrea Alaimo, Calogero Orlando, Stefano Valvano (2021). A preliminary Study on the Effect of Strut Waviness on the mechanical Properties of BCC Lattice unit Cells. ADM 2021 International Conference Design Tools and Methods in Industrial Engineering, 9th-10th September – Sapienza University of Rome (Italy).

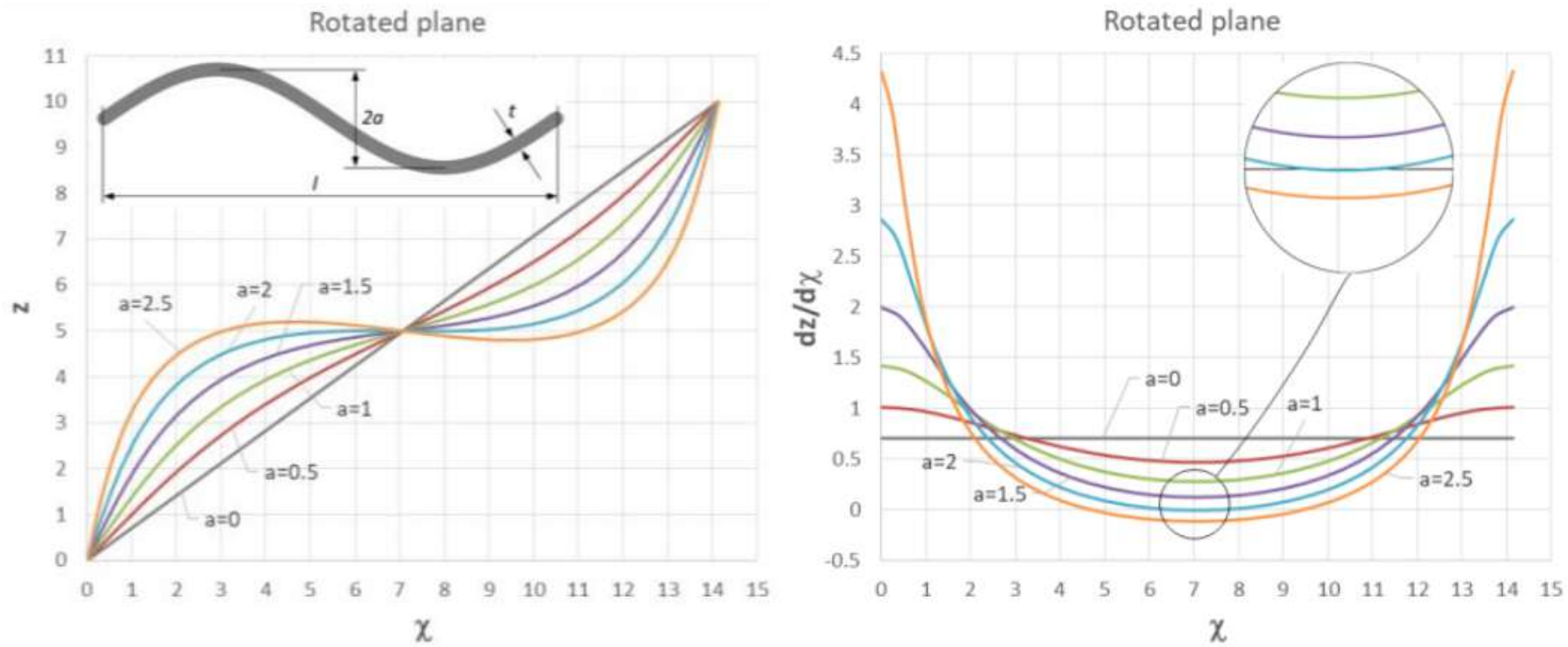

Fig. 3. Waved mid-axis of the struts in the rotated χ-z plane (left) and relative derivative (right), dimensions in [mm].

Davide Tumino, Andrea Alaimo, Calogero Orlando, Stefano Valvano (2021). A preliminary Study on the Effect of Strut Waviness on the mechanical Properties of BCC Lattice unit Cells. ADM 2021 International Conference Design Tools and Methods in Industrial Engineering, 9th-10th September – Sapienza University of Rome (Italy).

An empirical model has been defined by **Gibson and Ashby** to predict the mechanical stiffness of a generic cellular cell as a function of its relative density:

$$\frac{E^*}{E_s} = C\left(\frac{\rho^*}{\rho_s}\right)^2 \quad \text{for bending dominated cells}$$

$$\frac{E^*}{E_s} = C\left(\frac{\rho^*}{\rho_s}\right) \quad \text{for stretch dominated cells}$$

E^* is the modulus of the cellular structure,
E_s is the modulus of the bulk material,
ρ^* is the density of the cellular structure,
ρ_s is the density of the bulk material,
C is the Gibson-Ashby constant that depends on the unit cell geometry and topology and can be determined by experimental tests.

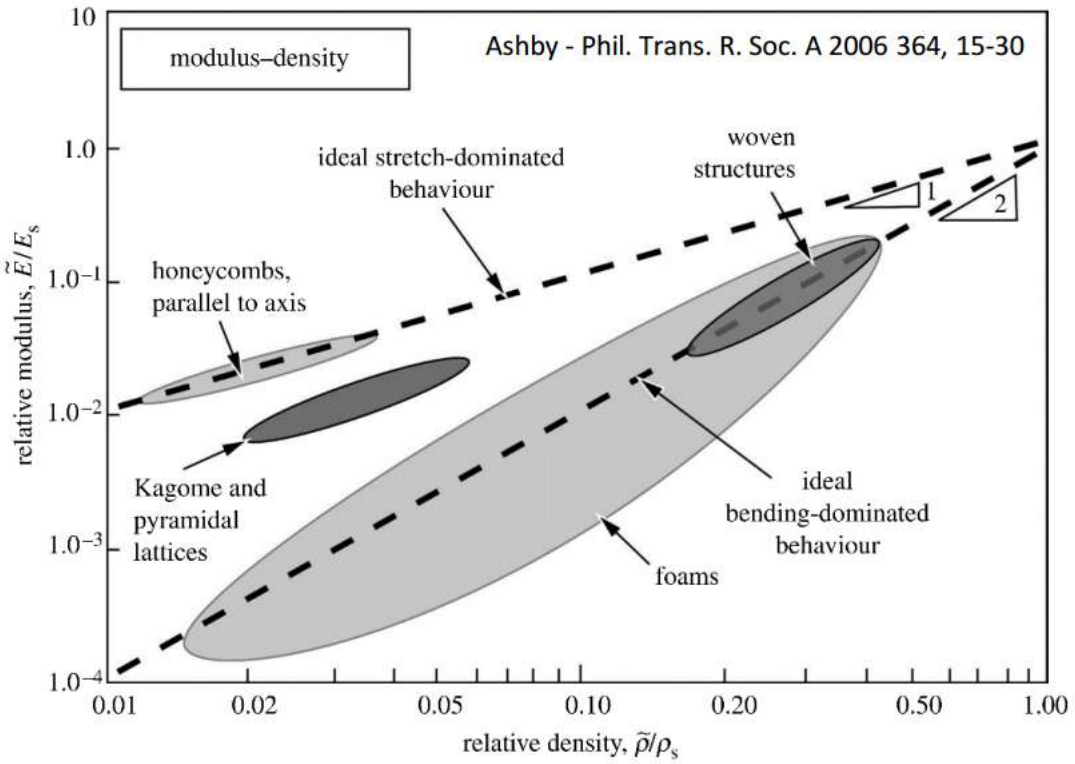

Davide Tumino, Andrea Alaimo, Calogero Orlando, Stefano Valvano (2021). A preliminary Study on the Effect of Strut Waviness on the mechanical Properties of BCC Lattice unit Cells. ADM 2021 International Conference Design Tools and Methods in Industrial Engineering, 9th-10th September – Sapienza University of Rome (Italy).

Linear periodic boundary condition

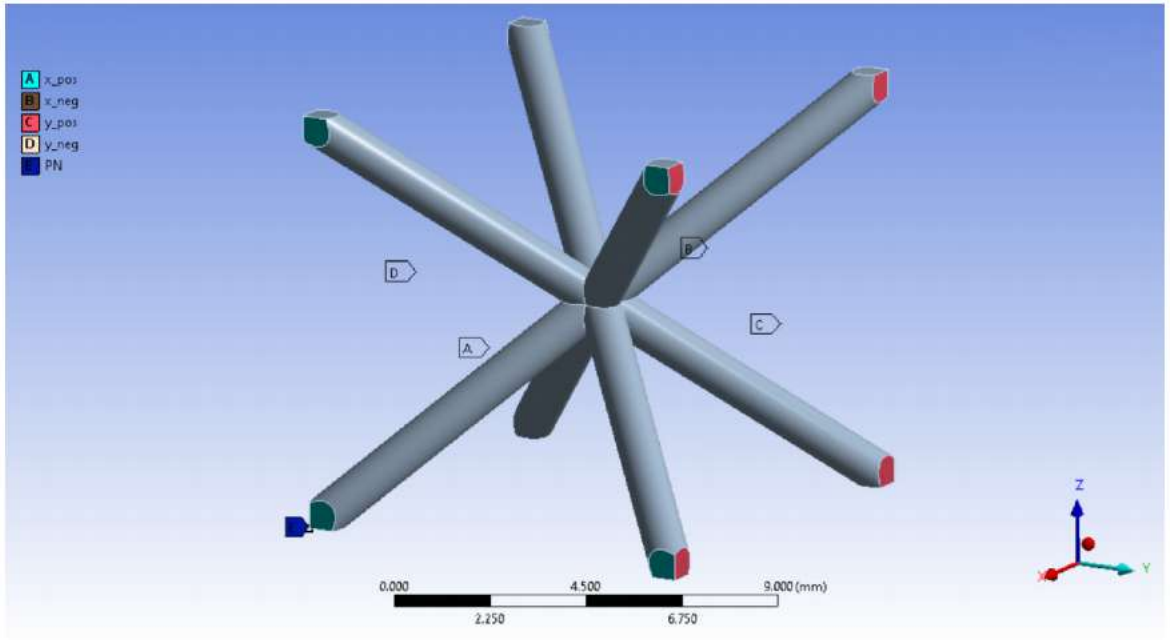

Figure 3. Applied linear periodic condition

$$X_{pos} = X_{neg} + X_{PN}$$
$$Y_{pos} = Y_{neg} + Y_{PN}$$

Alaimo A, Marino F, Valvano S (2021), ”BCC lattice cell structural characterization”, Reports in Mechanical Engineering 2(1): 77-85

Cell convergence analysis

$$Err(E_i) = \frac{E_i - E_{ref}}{E_{ref}} \cdot 100 \tag{15}$$

where $Err(E_i)$ is the error computed for the ith cells configuration and E_{ref} is the Young's modulus for the reference cells configuration.

Table 1. Relative errors for the convergence analysis about the cell's number in the Young and Poisson setups

Cell's number	E	Error(E) %	ν	Error(ν) %
3	1.1638E+09		0.44070	
2	1.1645E+09	0.057	0.44069	0.003
1	1.1385E+09	2.178	0.44125	0.124

Alaimo A, Marino F, Valvano S (2021), "BCC lattice cell structural characterization", Reports in Mechanical Engineering 2(1): 77-85

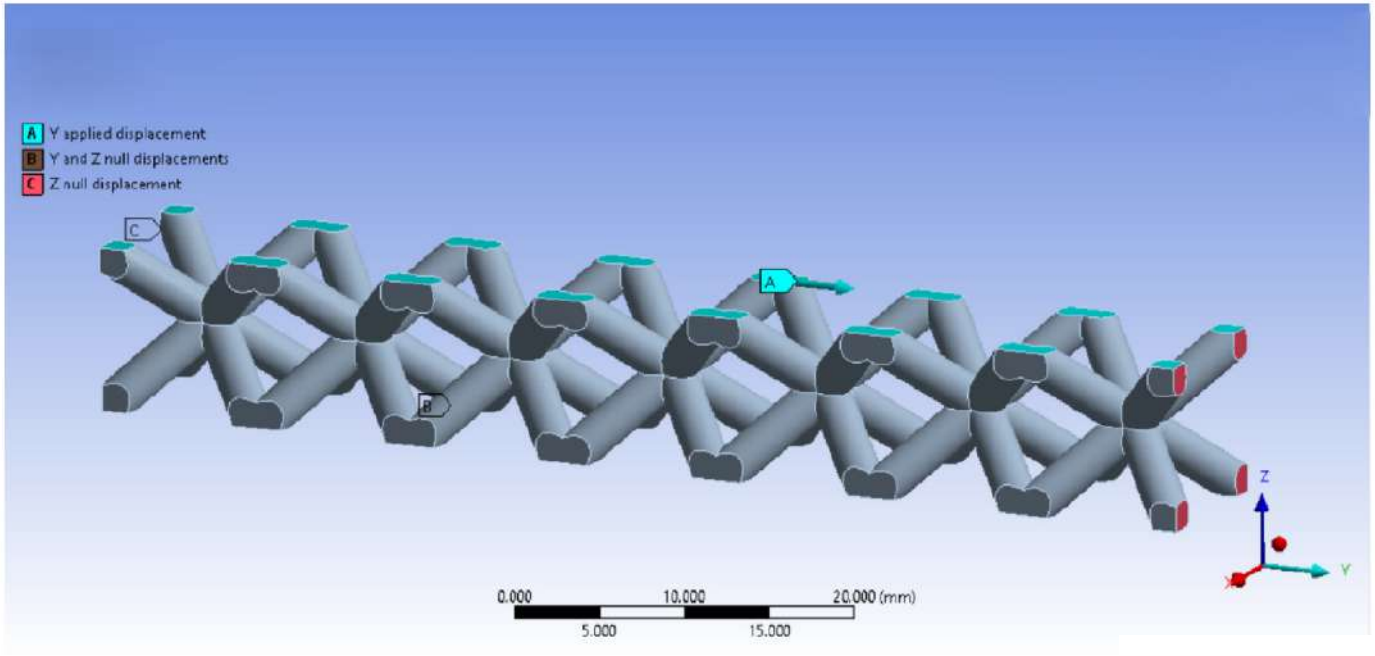

Figure 5. Shear load condition

Table 2. Relative errors for the convergence analysis about the cell's number in the shear setup

Cell's number	G	Error(G) %
7	2.5229E+09	
6	2.4573E+09	2.597
5	2.3664E+09	6.202
4	2.2305E+09	11.590
3	2.0121E+09	20.244
2	1.6343E+09	35.220
1	1.1385E+09	54.873

Alaimo A, Marino F, Valvano S (2021), ”BCC lattice cell structural characterization”, Reports in Mechanical Engineering 2(1): 77-85

Uni-axial compression tests (Young modulus)

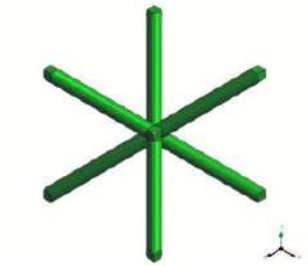

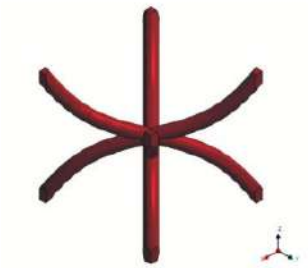

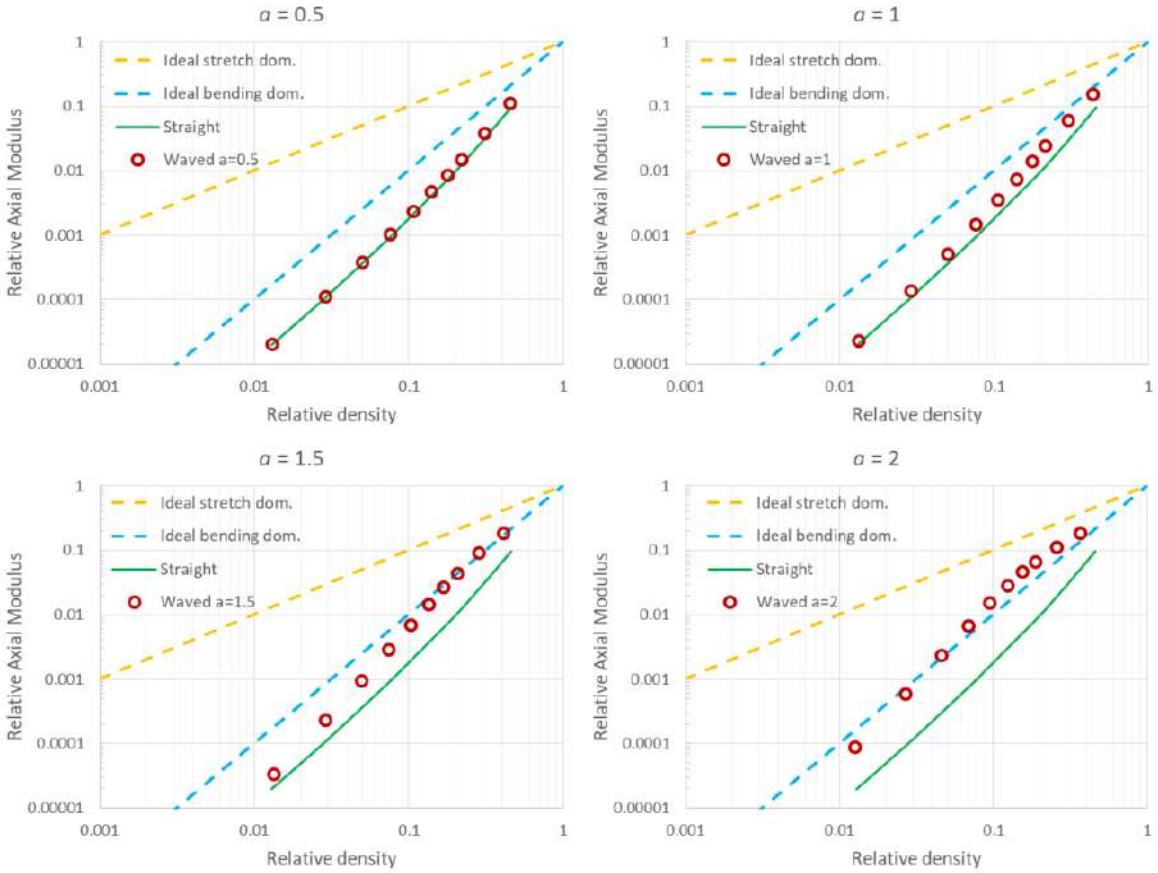

Davide Tumino, Andrea Alaimo, Calogero Orlando, Stefano Valvano (2021). A preliminary Study on the Effect of Strut Waviness on the mechanical Properties of BCC Lattice unit Cells. ADM 2021 International Conference Design Tools and Methods in Industrial Engineering, 9th-10th September – Sapienza University of Rome (Italy).

Uni-axial compression tests (Poisson coefficient)

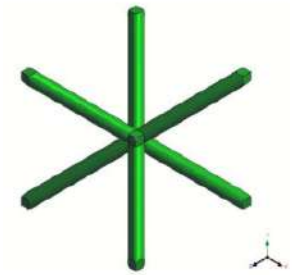

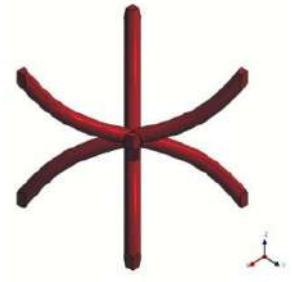

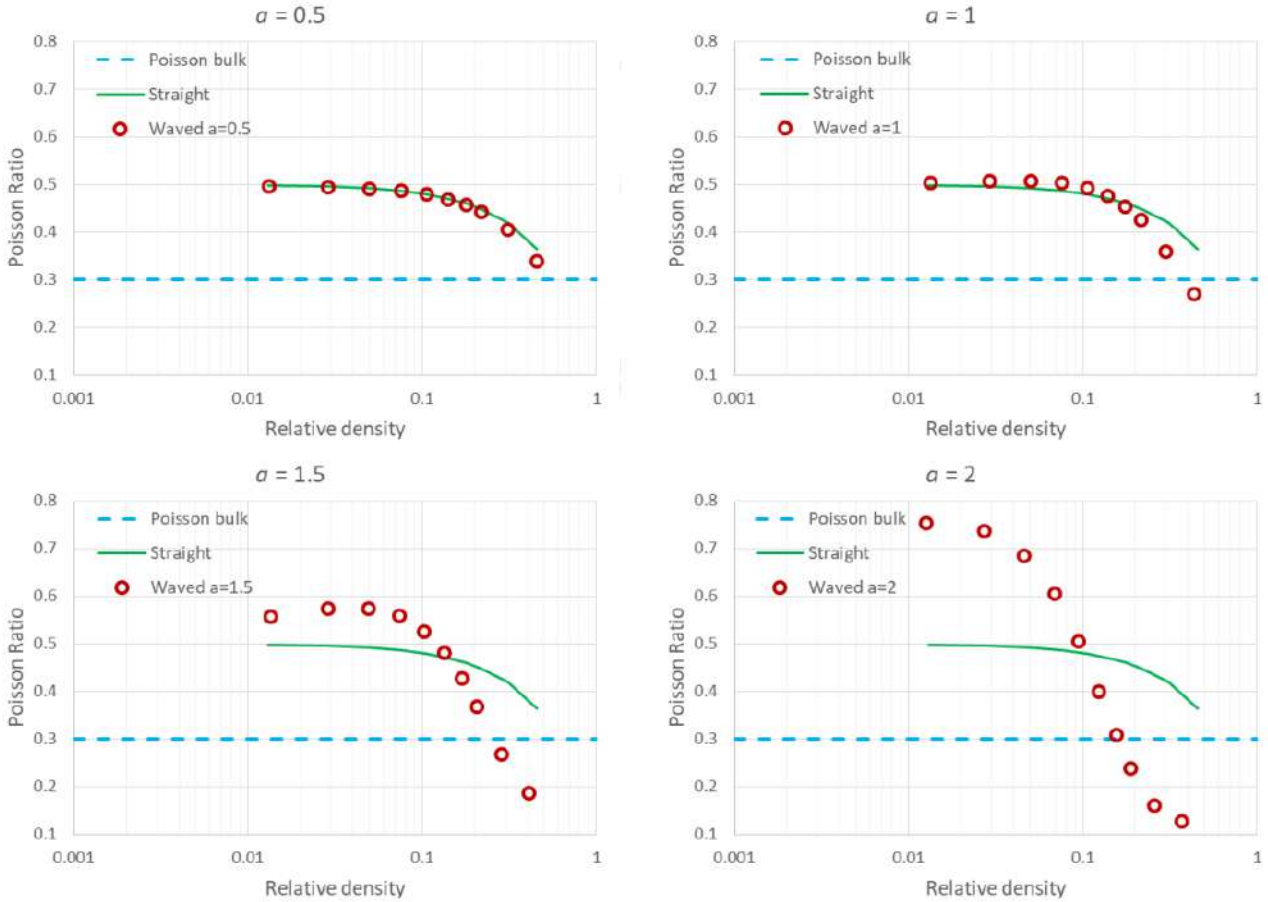

Davide Tumino, Andrea Alaimo, Calogero Orlando, Stefano Valvano (2021). A preliminary Study on the Effect of Strut Waviness on the mechanical Properties of BCC Lattice unit Cells. ADM 2021 International Conference Design Tools and Methods in Industrial Engineering, 9th-10th September – Sapienza University of Rome (Italy).

In-plane shear tests (Shear modulus)

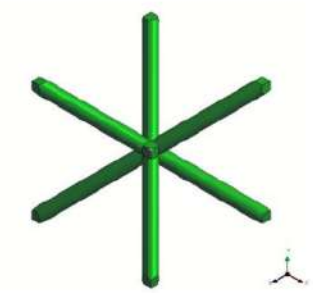

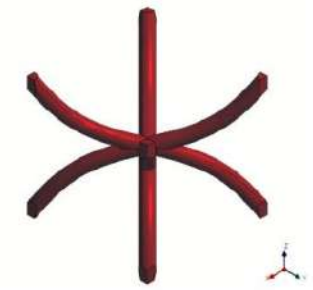

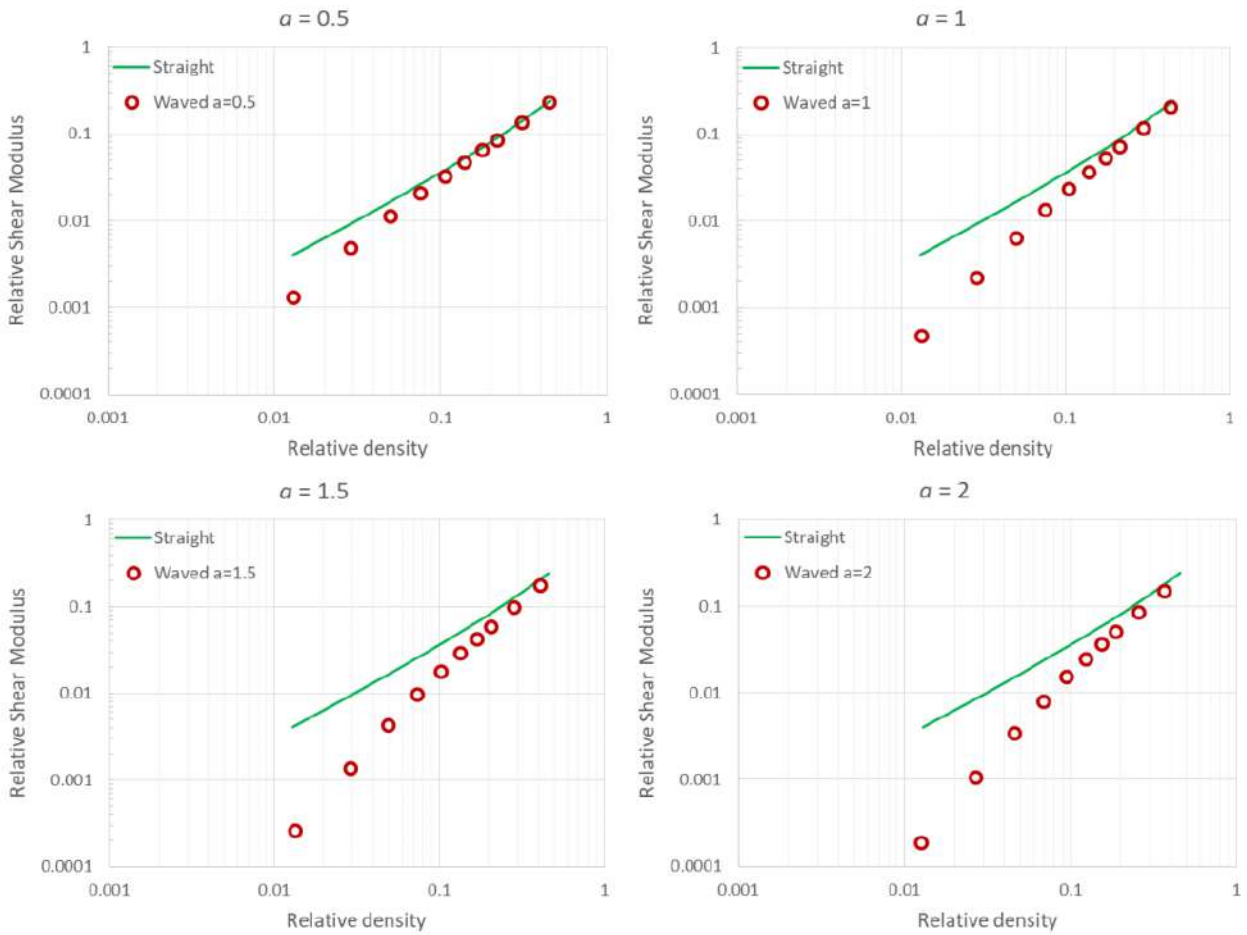

Davide Tumino, Andrea Alaimo, Calogero Orlando, Stefano Valvano (2021). A preliminary Study on the Effect of Strut Waviness on the mechanical Properties of BCC Lattice unit Cells. ADM 2021 International Conference Design Tools and Methods in Industrial Engineering, 9th-10th September – Sapienza University of Rome (Italy).

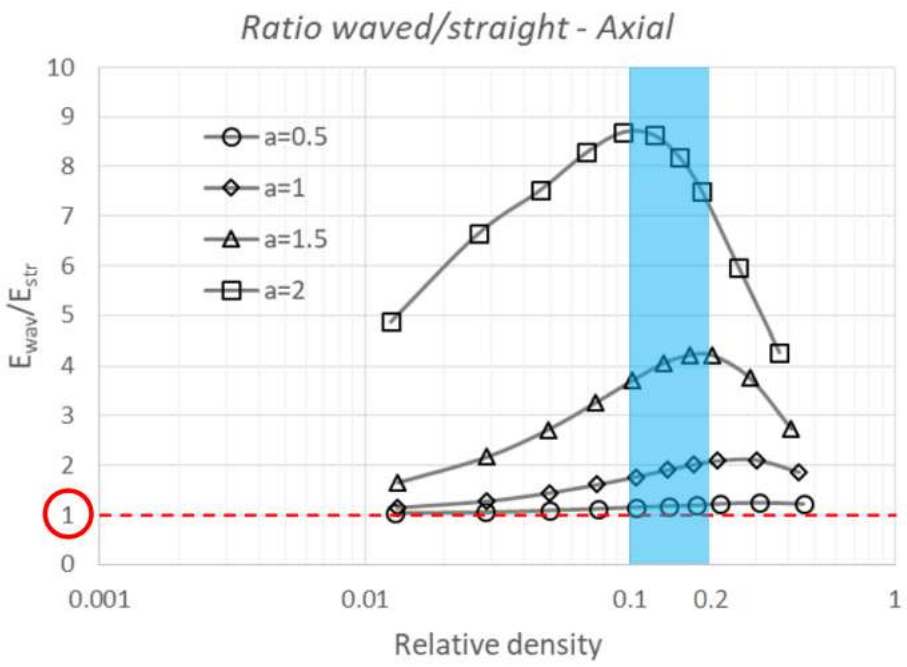

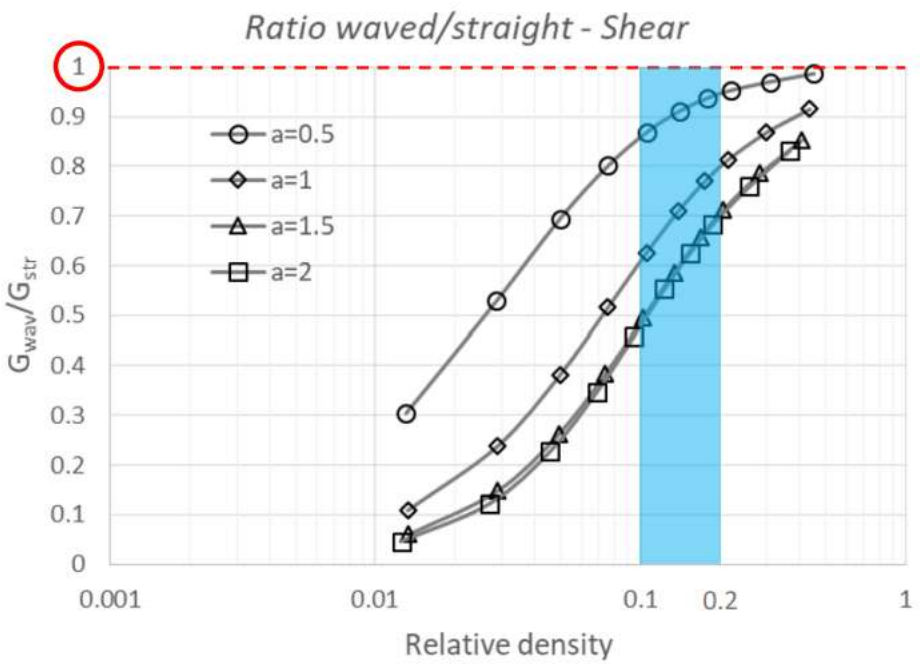

The clear blue interval corresponds to the typical relative density used for commercial lattice structures.

Davide Tumino, Andrea Alaimo, Calogero Orlando, Stefano Valvano (2021). A preliminary Study on the Effect of Strut Waviness on the mechanical Properties of BCC Lattice unit Cells. ADM 2021 International Conference Design Tools and Methods in Industrial Engineering, 9th-10th September – Sapienza University of Rome (Italy).

Conclusions

1. The study of the sound transmission through aircraft fuselage sections confirmed the importance of the fuselage panels layup design in order to reduce the noise received inside the fuselage.

2. The main acoustic parameters for the sound transmission analysis are the sound pressure field and the transmitted sound power, both dependent on the vibrational velocity distribution of the fuselage inner surfaces.

3. For the evaluation of the vibrational velocity distribution of the fuselage panels, it is necessary to perform frequency-response analysis of the considered fuselage panels structures.

4. In order to get accurate structural results, without huge computational costs, it is mandatory to use 2D shell kinematic models for the analysis of aircraft fuselage panels.

Conclusions

5. The design study of the fuselage panels, for the noise reduction analysis, is focused on the layout configuration of sandwich panels with advanced materials, e.g. composite, viscoelastic, lattice.

6. In order to get accurate results for the analysis of classical metallic sandwich panels, it is mandatory to consider higher-order 2D theories with zig-zag capabilities.

7. In order to characterize the viscoelastic behavior of soft materials and to include it in the 2D theories, it is preferable to adopt fractional derivative models with four or five material parameters.

8. Considering the frequency-response analysis of multilayered composite sandwich structures with viscoelastic core, it is mandatory to use layer-wise 2D higher-order models to reach accurate results.

Conclusions

9. In order to improve and push forward the tailoring of the sandwich panels, the use of additive manufacturing processes permits to use lattice structures for the sandwich cores.

10. In order to analyze the global response of the fuselage panels and to avoid to increase the computational costs, it is important to properly consider, in the 2D shell models, the lattice materials as an homogenized material.

11. The structural properties of an unit lattice cell can be tailored controlling different parameters, e.g. the struts diameter, the struts waviness, etc. etc..

Conclusions

- **It is clear that in a design process of a multilayered shell panels there are so many parameters that a proper choice is not an easy task.**
- **An optimization study should be mandatory in order to well design the aircraft fuselage panels.**